University of Zurich[UZH]

Quantifying the contributions to discharge of snow and glacier melt

D. FREUDIGER, M. VIS AND J. SEIBERT

IM AUFTRAG DES BUNDESAMTES FÜR UMWELT BAFU – JANUAR 2021

EIN FORSCHUNGSPROJEKT IM RAHMEN DES NCCS THEMENSCHWERPUNKTES "HYDROLOGISCHE GRUNDLAGEN ZUM KLIMAWANDEL" DES NATIONAL CENTER FOR CLIMATE SERVICES

Impressum

Commissioned by: Federal Office for the Environment (FOEN), Hydrology Division, CH-3003 Bern. The FOEN is an agency of the Federal Department of the Environment, Transport, Energy and Communications (DETEC).

Contractor: University of Zürich, Institute of Geography, Winterthurerstrasse 190, CH-8056 Zürich

Authors: Daphné Freudiger, Marc Vis, Jan Seibert

FOEN support: Fabia Huesler, Petra Schmocker-Fackel

Citation: D. Freudiger, M. Vis, and J. Seibert, 2020. Quantifying the contributions to discharge of snow and glacier melt. Hydro-CH2018 project. Commissioned by the Federal Office for the Environment (FOEN), Bern, Switzerland, 49 pp.

Summary

Switzerland is often referred to as Europe's water tower. Freshwater stored in form of snow and ice is released during the melt season to feed large European rivers such as the Rhine and the Rhone rivers. Under climate change conditions, change in precipitation behavior, and increased temperatures will induce dramatic changes of the rain, snow and glacier melt contributions to discharge and therefore influence the seasonality of total discharge. Understanding how much meltwater contributes to discharge in Swiss glacierized headwater catchments under different climate change scenarios is therefore essential for assessing water availability in the future for sustainable water management of our water resources.

As part of the Hydro-CH2018 project, this study aims to assess the daily contribution of rain, snow and glacier melt to discharge transiently. We use a customized version of the bucket-type hydrological model software, HBV-light, which was specially developed to track the discharge components. The discharge components were simulated from 1973 to 2099 for 190 glacierized and 5 non-glacierized headwater catchments covering the entire Swiss Alps. Discharge modelling in alpine catchments is challenging, on the one hand, due to the high spatial and temporal variability of the hydrological processes and, on the other hand, due to the data scarcity and heterogeneous distribution of the few measurement stations. As model input data for future climate projections, we used the newly generated precipitation and temperature gridded products from the National Center for Climate Services (NCCS, CH2018) for 45 climate model runs and three emissions scenarios (RCP 2.6, RCP 4.5 and RCP 8.5). We show the advantages of using combined datasets of various sources, such as discharge measurements, remotely sensed regional snow elevation line, interpolated snow water equivalent, and glacier volume changes for multi-criteria model calibration. This calibration approach ensured that all hydrological processes were correctly represented by the model. For the ungauged catchments (157), we applied a regionalization approach for defining the model parameters.

While annual total discharge might only marginally change under climate change conditions, the single discharge components will experience large changes that differ spatially. The simulation results show that glacier peak water is already reached by most of the catchments and will be reached by all catchments during the first half of the century for all three emissions scenarios. Total glacier contribution summarized over all headwater catchments is 7% of total discharge under current climate and expected to be less than 2% at the end of the century under all climate scenarios. In all river basins and under all emission scenarios, the rain component represents ca. 57% of total discharge under current climate and is expected to increase until the end of the century. The snowmelt contribution to discharge shows the largest differences between emission scenarios RCP 2.6 and RCP 8.5 and represents a significant part of the total discharge, in particular at high altitudes. With an average contribution of 35% under current climate, snowmelt contribution will decrease by 6 and 19 percentage units under RCP 2.6 and RCP 8.5, respectively. However, large regional differences exist. The changes in the contribution of rain, snow and glacier melt to total discharge will lead to a shift of the discharge seasonality with annual maximum occurring earlier in the year due to earlier snowmelt events. The discharge peaks are also expected to become smaller, due to negative changes in snowmelt and glacier melt contribution to discharge. The intensity of the changes in discharge contributions depends on the catchment elevation, and glacier cover and large regional differences are expected.

Zusammenfassung

Die Schweiz wird oft als das Wasserschloss Europas bezeichnet. Das in Form von Schnee und Eis gespeicherte Süsswasser wird während der Schmelze freigesetzt und speist grosse europäische Flüsse, vor allem Rhein und Rhone. Aufgrund des Klimawandels werden steigende Temperaturen sowie räumliche und zeitliche Veränderungen in der Niederschlagsverteilung erwartet. Dies wird zu Veränderungen der Beiträge von Regen, Schnee- und Gletscherschmelze am Abfluss führen und damit die Saisonalität des gesamten Abflusses beeinflussen. Für ein angepasstes Wassermanagement ist daher ein gutes Verständnis darüber, wie viel Schmelzwasser unter der Annahme der verschiedenen Klimawandelszenarien zum Abfluss in schweizerischen vergletscherten Kopfeinzugsgebieten beiträgt, wichtig, um die zukünftigen Wasserverfügbarkeit der Wasserressourcen beurteilen zu können.

Diese Studie, die im Rahmen des Hydro CH-2018-Projekts durchgeführt wurde, hatte zum Ziel, die täglichen Beiträge von Regen sowie Schnee- und Gletscherschmelze zu dem sich veränderenden Abfluss zu quantifizieren. Dazu wurde das einfache hydrologische Abflussmodell HBV in der Version HBV-light verwendet. Diese Modellversion wurde speziell weiterentwickelt, um zu ermöglichen, dass ier Abflusskomponenten durch das Modell verfolgt werden können. Die Abflusskomponenten wurden für den Zeitraum 1973 bis 2099 für 190 vergletscherte und 5 nicht vergletscherte Kopfeinzugsgebiete, die zusammen die gesamten Schweizer Alpen abdecken, simuliert. Die Abflussmodellierung in alpinen Einzugsgebieten ist eine Herausforderung, einerseits wegen der hohen räumlichen und zeitlichen Variabilität der hydrologischen Prozesse und andererseits wegen der begrenzten Datengrundlage sowie der ungleichen Verteilung der wenigen Messstationen. Als Modelleingangsdaten für zukünftige Klimaprojektionen verwendeten wir die neuen Niederschlags- und Temperatur-Rasterprodukte des National Center for Climate Services (NCCS, CH2018) für 45 Klimamodelläufe und drei Emissionsszenarien (RCP 2.6, RCP 4.5 und RCP 8.5). Die Kombination verschiedener Daten, wie Abflussmessungen, regionale Schneehöhenlinien aus Fernerkundungsdaten, Interpolationen des Schneewasseräquivalents aus Punktmessungen und Gletschervolumenänderungen, war wichtig für eine gute Modellkalibrierung. Diese Vorgehensweise zur Kalibrierung stellte sicher, dass alle hydrologischen Prozesse durch das Modell so realistisch wie möglich dargestellt wurden. Für die nicht kalibrierten Einzugsgebiete (157) verwendeten wir einen Regionalisierungsansatz zur Abschätzung der Modellparameterwerte.

Unsere Ergebnisse deuten darauf hin, dass sich der gesamte mittlere jährliche Abfluss unter den Bedingungen des Klimawandels nur geringfügig ändern wird. Für die einzelnen Abflusskomponenten sind jedoch grosse Veränderungen und räumliche Variationen zu erwarten. Der grösste Beitrag der Gletscherschmelze, das sogenannte ‚peak water', wurde bereits von den meisten Einzugsgebieten erreicht und wird in der ersten Hälfte des Jahrhunderts für alle drei Emissionsszenarien in allen Einzugsgebieten überschritten werden. Unter den gegenwärtigen Klimabedingungen beträgt der Gesamtbeitrag der Gletscherschmelze für alle Kopfeinzugsgebiete insgesamt 7% des Gesamtabflusses. Für alle drei Emissionsszenarien wird dieser Anteil bis zum Ende des Jahrhunderts auf weniger als 2% sinken. In allen untersuchten Einzugsgebieten trägt die Regenkomponente zu etwa 57% des Gesamtabflusses unter den gegenwärtigen Klimabedingungen bei, und wird den Berechnungen nach bis zum Ende des Jahrhunderts zunehmen. Der Beitrag der Schneeschmelze zum Abfluss unterscheidet sich deutlich zwischen den Emissionsszenarien RCP 2.6 und RCP 8.5. Bei einem durchschnittlichen Beitrag von 35% unter den gegenwärtigen Klimabedingungen wird der Beitrag der Schneeschmelze unter RCP 2.6 und RCP 8.5 um 6 beziehungsweise 19 Prozentpunkte abnehmen. Es bestehen jedoch grosse regionale Unterschiede. Die Veränderungen der Bedeutung von Regen sowie Schnee- und Gletscherschmelze zum Gesamtabfluss werden zu einer Verschiebung der Abflusssaisonalität führen, wobei das jährliche Maximum aufgrund der zeitlich verschobenen Schneeschmelze früher im Jahr eintritt. Es wird auch erwartet, dass die jährlichen Abflussspitzen aufgrund der Abnahme der Beiträge von Schnee- und Gletscherschmelze kleiner werden. Der Umfang der Veränderungen der Abflussbeiträge hängt von der Höhe des Einzugsgebiets und der Gletscherbedeckung ab, und grosse regionale Unterschiede sind zu erwarten.

Résumé

La Suisse est souvent considérée comme le château d'eau de l'Europe. L'eau douce, accumulée sous forme de neige et de glace, est libérée lors de la fonte pour alimenter les grands fleuves européens comme le Rhin et le Rhône. Dans des conditions de changement climatique, la modification de la saisonnalité des précipitations et l'augmentation des températures induiront des changements importants dans la contribution au débit de la pluie, de la fonte des neiges et des glaces, ce qui influencera la saisonnalité du débit total. Il est donc essentiel de comprendre dans quelle mesure les eaux de fonte contribuent au débit dans les bassins versants des glaciers suisses selon différents scénarios de changement climatique pour évaluer la disponibilité de l'eau en vue d'une gestion durable de nos ressources.

Cette étude, qui fait partie intégrante du projet Hydro-CH2018, vise à évaluer la contribution quotidienne de la pluie, de la neige et de la fonte des glaciers au débit total dans le climat actuel et futur. Nous utilisons une version améliorée du logiciel de modélisation hydrologique, HBV-light, qui a été spécialement développé pour suivre les différentes composantes de l'écoulement (pluie, fontes des neiges et des glaces) le long des cours d'eau. Les composantes du débit ont été simulées de 1973 à 2099 pour 190 bassins versants avec glaciers et 5 sans, couvrant l'ensemble des Alpes suisses. La modélisation des débits dans les bassins versants alpins est un défi, d'une part, en raison de la grande variabilité spatiale et temporelle des processus hydrologiques et, d'autre part, en raison de la rareté des données et de la distribution hétérogène des quelques stations de mesure. Pour les simulations de projections climatiques, nous avons utilisé les nouveaux produits de précipitations et de températures du Centre National des Services Climatiques (NCCS, CH2018) consistants en 45 simulations de modèles climatiques pour trois scénarios d'émissions (RCP 2.6, RCP 4.5 et RCP 8.5). Dans cette étude, Nous montrons les avantages de l'utilisation combinée de données provenant de sources diverses pour une calibration multi-critérielle du modèle. Ces données proviennent de mesures de débit, de la ligne moyenne d'élévation de la neige (à partir de produits satellites), d'un produit d'interpolation d'équivalents en eau de la neige, ainsi que des changements de volume des glaciers. Cette approche a permis de s'assurer que tous les processus hydrologiques étaient correctement représentés par le modèle. Pour les bassins versants où aucunes mesures de débit n'étaient disponibles (157), nous avons appliqué une méthode de régionalisation pour définir les paramètres du modèle.

Alors que le débit total annuel pourrait ne changer que marginalement dans des conditions de changement climatique, les composantes individuelles, telles que la contribution provenant de la pluie ou de la fonte des neiges et des glaces, connaîtront de grands changements avec de larges différences régionales. Les résultats de la simulation montrent que le niveau maximal de débit provenant de la fonte des glaciers est déjà atteint pour la plupart des bassins versants et qu'il le sera pour tous les bassins versants au cours de la première moitié du siècle quel que soit le scénario d'émissions. Dans tous les scénarios d'émissions, la contribution totale des glaciers (la somme provenant de tous les bassins versants) est de 7% du débit total dans le climat actuel et sera de moins de 2% à la fin du siècle. Pour tous les bassins versants et selon tous les scénarios d'émissions, la composante pluie représente environ 57% du débit total dans le climat actuel et devrait largement augmenter d'ici la fin du siècle. La contribution de la fonte des neiges au débit présente les plus grandes différences entre les scénarios d'émission RCP 2.6 et RCP 8.5 et représente une part importante du débit total, en particulier en haute altitude. Avec une contribution moyenne de 35% dans le climat actuel, la contribution de la fonte des neiges diminuera de -6 et de -19 unités de pourcentage selon les scénarios RCP 2.6 et RCP 8.5. Il existe toutefois de grandes différences régionales. Finalement, les changements dans la contribution de la pluie et de la fonte des neiges et des glaces entraîneront un changement de la saisonnalité du débit, le maximum annuel se produisant plus tôt dans l'année en raison de la fonte précoce de la neige. On s'attend également à ce que les pics de débit deviennent plus faibles, en raison de la diminution de la contribution de la fonte des neiges et des glaces comparée à la période de référence. Cependant, l'intensité des changements dans les contributions au débit dépend de l'altitude du bassin versant et de la couverture glaciaire, par conséquent, de grandes différences régionales sont attendues.

Table of contents

List of Figures

List of Tables

List of abbreviations

A	Area
AMRE	Absolute Mean Relative Error, performance criterion for glacier volume change simulation
CH2018	Swiss climate change scenarios
DEM	Digital Elevation Model
dP	Precipitation-elevation gradient
dT	Temperatur-elevation gradient
FOEN	Federal Office of the Environment
HADES	Hydrological Atlas of Switzerland
HBV-light	Semi-distributed hydrological model to simulate catchment runoff
Hydro-CH2018	Ensemble of research projects funded bei FOEN with the aim to improve understanding of the impact of climate change on water resources in Switzerland
MANE	Mean Absolute Normalized Error, performance criterion for SWE simulation
m asl	Meter above sea level
NCCS	National Center for Climate Services
P	Precipitation
PET	Evapotranspiration
Q_{tot}, Q_{Rain}, Q_{Snow}, Q_{Ice}	Total discharge and discharge components from rain, snow and glacier melt
R_{Qi}, R_{SCA}, R_{SWE}, R_G	Evaluation criteria for model calibration on discharge, snow and glacier cover
RCP	Representative Concentration Pathways – emissions scenarios for future climate
RMSE	Root Mean Square Error, performance criterion for SCA simulation
RSLE	Regional Snowline Elevation
SCA	Snow Covered Area
SLF	WSL Institute for Snow and Avalanche Research
SWE	Snow Water Equivalent
T	Temperature
V	Volume
WSL	Swiss Federal Institute for Forest, Snow and Landscape Research

1. Introduction

The Alps are often called water tower of Europe, thanks to the large amounts of water stored in the form of ice and snow at high altitudes. Alpine discharge is highly seasonal and is characterized by low flow in winter, strong snowmelt events in spring and glacier melt driven discharge peaks in summer. Additionally, glaciers can reduce the interannual variability in discharge as they store water during the wet cold years and release it during the dry warm years (e.g. Koboltschnig *et al.*, 2007; Viviroli *et al.*, 2011). Until the end of the century and under climate change conditions, the discharge regime is expected to change in glacierized catchments. The annual precipitation sum is expected to increase until the end of the century with increased precipitation amounts in winter and decreased precipitation amounts in summer (CH2018, 2018). The overall increase of temperature will lead to reduced snowfall fractions, meaning an increase in rainfall with some differences depending on the elevation (CH2018, 2018). Alpine snow cover is therefore expected to change with lower snow accumulation and a shift in the timing of the snowmelt (Serquet *et al.*, 2011; De Vries, Lenderink and Van Meijgaard, 2014; Frei *et al.*, 2018; CH2018, 2018). However, the combined effect of increased temperatures and increased winter precipitation might induce stable or even increased snowfall in winter at the highest elevations in some regions (CH2018, 2018). Finally, European glaciers are expected to largely or even completely retreat until the end of the century as a response to a warming climate (e.g. Salzmann, MacHguth and Linsbauer, 2012; Huss and Hock, 2018; Zekollari, Huss and Farinotti, 2019), losing a total volume of up to 80% +/- 15% (Huss *et al.*, 2017), with large regional differences in their response time mainly depending on glacier specific characteristics such as glacier slope or elevation range (Huss and Fischer, 2016; Zekollari, Huss and Farinotti, 2020). Combining all these changes may have a strong impact on the alpine discharge regime that is, nowadays, not fully understood (Beniston *et al.*, 2018). Assessing how rain, snow and glacier melt contribute to discharge is essential for sustainable management of our water resources in future.

Changes in seasonality of the total discharge have already been pointed out in observed time series in alpine river basins for the recent past (Belz *et al.*, 2007; Bard *et al.*, 2015) and analysed in discharge simulations in many alpine catchments for present and future climate (e.g. Farinotti *et al.*, 2012; Addor *et al.*, 2014; Stahl *et al.*, 2016; Etter *et al.*, 2017; Brunner *et al.*, 2019). Glacier and snow cover changes were often related to the changes in total discharge, but only a few studies modelled explicitly the contribution to discharge of the different discharge components. Weiler, Seibert and Stahl (2018) pointed out the necessity to assess the discharge components to understand changes in future total discharge and the challenges linked to the component tracking in hydrological models. To understand how the different discharge components impact the total discharge at the medium to large scale, they argue that hydrological models should be able to track the effect of the different discharge contributions (meaning the representation of the signal of rainfall, snow and glacier melt in discharge downstream – fast response) rather than to track the water particles (for example in the form of isotopes – slow response, especially in the presence of water reservoirs such as lakes).

Meltwater contribution to discharge is particularly important during drought events and can impact discharge far downstream. Few model-based studies have tracked the effect of the contribution of glacier melt runoff as well as snowmelt runoff during drought events, such as the summers 1921, 1979, or 2003 (Koboltschnig *et al.*, 2007; Huss, 2011; Stahl *et al.*, 2017). Stahl et al. (2017), for example, found out that glacier melt was an important contribution to discharge in the entire Rhine River basin during the drought summer 2003, and its simulated contribution was even significant in Lobith (the Netherlands) for several days. These studies on historical runoff show, on the one hand, the importance of meltwater contribution to discharge under extreme climatic conditions. On the other hand, they show the necessity of simulations with a daily time step, as melt events may also matter at short time scales. The semi-distributed bucket-type hydrological model HBV-light (Seibert et al., 2012), used in this study, has been specially enhanced to track the effect of the daily contribution of rainfall, snow and glacier melt to discharge transiently in Swiss alpine catchments (Stahl et al., 2016). It has been successfully used to assess changes in the different discharge components for the past between 1901 and 2006 in the Rhine River catchment (Stahl et al., 2016).

Assessing discharge in the Alps is challenging due to the scarcity of hydrological and meteorological measurement data at high altitudes - due to extreme conditions. Furthermore, the meteorological conditions in the Alps are spatially highly variable, mainly due to topography, making measurement stations only little representative for larger areas (e.g. Frei and Schär, 1998; Schädler and Weingartner, 2002). The use of

meteorological gridded datasets, based on the interpolation of station data, for hydrological modelling was proved to be a valuable alternative to station data for large scale hydrological modelling in alpine catchments to catch the spatial variability of climate and get along with data scarcity (e.g. Freudiger *et al.*, 2016). Such products are widely used in hydrological studies. Furthermore, spatially distributed modelled or interpolated products on snow water equivalent (SWE) or glacier cover and remotely sensed information on snow and glacier cover exist nowadays, which enable robust model calibration on different aspects of the hydrograph. Calibration of hydrological models on multiple criteria is essential to ensure that all hydrological processes are correctly represented by the model, especially in high elevated and glacierized catchments (e.g. Seibert, 2000; Konz and Seibert, 2010; Finger *et al.*, 2015; Van Tiel *et al.*, 2020). This is especially important to ensure accurate modelling of the different discharge components.

This study is part of the Hydro-CH2018 project to assess all aspects of the changes in water resources under future climate conditions in Switzerland (see BAFU, 2021). This study aims to use what we learnt from the quantification of rain, snow and ice melt components for the *past* in the Rhine River basin (ASG1-project, Stahl et al., 2016) to update the quantification for the *present* and, most importantly, to predict changes for the *future* for all Swiss glacierized headwater catchments of the Inn, Ticino, Rhine and Rhone River basins. We estimate the discharge components for 190 glacierized and 5 non-glacierized headwater catchments covering the entire Swiss Alps from 1973 to 2099 using the semi-distributed bucket-type HBV model in the software implementation HBV-light. We first show the advantages and challenges of using datasets from various sources as meteorological input data and for model calibration and validation of discharge, snow and glacier cover information. In a second step, we apply a regionalization approach to define model parameters for the ungauged catchments. A multi-criteria calibration is used to ensure that all hydrological processes are correctly represented within the model. Finally, we analyze and discuss the changes in the discharge components rain, snow and ice melt until the end of the century. By this, we contribute to a better understanding of the changes in seasonality and interannual variability of total discharge in future and the data can help to identify potential risks for extreme streamflow events, especially low flow conditions, in a changing climate.

2. Methods and Data

To estimate the rainfall, snow and ice melt contribution to discharge for future climate scenarios, we used the bucket-type hydrological model HBV-light (Seibert and Vis, 2012), from which the snow and glacier modules were especially developed for long-term modelling in alpine regions during the ASG1-project (Stahl *et al.*, 2016; Seibert *et al.*, 2017). Furthermore, the effect tracking of the discharge components was implemented to separate the water coming from rainfall, snow and ice melt in the total discharge (Stahl *et al.*, 2016; Weiler, Seibert and Stahl, 2018).

In Figure 1, the methodology followed to estimate the discharge components is schematically represented. The HBV-light model mainly needs precipitation, temperature and catchment characteristics (elevation, aspect, glacier cover at the start of the simulation) as input. To best estimate the discharge, the model needs to be calibrated on observations. The numerous benefits of multi-criteria calibration using diverse observation datasets to calibrate hydrological models have often been demonstrated (e.g., Seibert, 2000; Seibert and McDonell, 2002; Konz and Seibert, 2010), especially in high-elevated and glacierized catchments (Finger et al., 2015; Van Tiel et al., 2020). HBV-light was therefore first calibrated using current meteorological input data and a combination of discharge, glacier and snow cover observations. A description of all data used as model input or for calibration purposes can be found in Table 1 and in Section 2. The modelled headwater catchments were delineated based on data availability, discharge observations and glacier cover (Section 2.1). The model calibration was performed differently for gauged and ungauged catchments for the period 1973-2017 (preceded by 3 years of model warm-up). First, the gauged catchments were calibrated on all available observations. Then the calibrated parameter sets were transferred to the ungauged catchments using a regionalization approach. Finally, the ungauged catchments were re-calibrated on snow and glacier cover information. The multi-criteria calibration processes and the regionalization are presented in Section 4.1 (for gauged catchments) and 4.2 (for ungauged catchments).

Once the model was successfully calibrated on the current climate, the model was run for several climate scenarios (see Section 2.3 and Section 4) using the calibrated parameter sets. The computed discharge components were then analyzed for changes in Section 5.

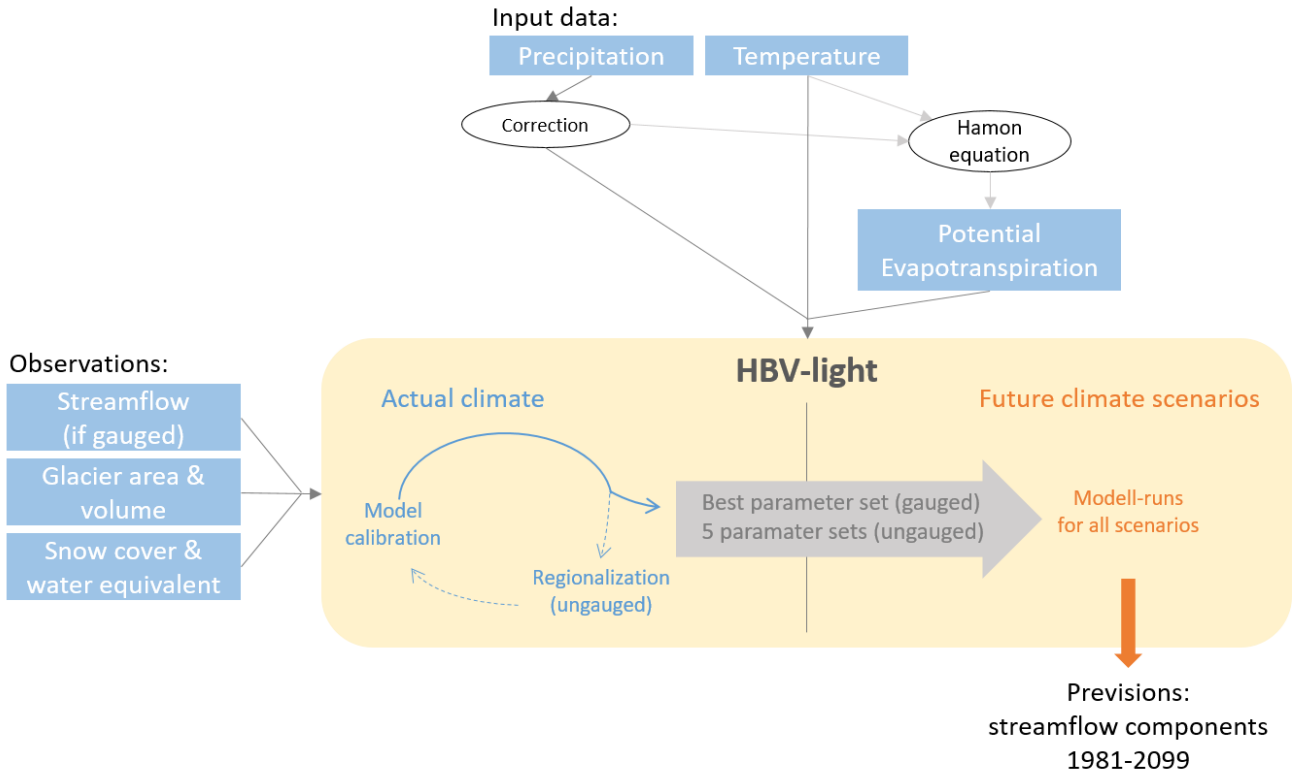

Figure 1: Schematic representation of the methodology.

Table 1: List of all data used as model input and for model calibration.

Dataset	Data	Resolution	Provider	Time period	Comment
Snow water equivalent	SWE (mm)	daily mean, gridded product 1x1km	SLF	1998-2018	from phys. based model and interpolation
Snow elevation line	RSLE (m asl)	daily mean, catchment mean	S. Fugger	2002-2018	Snow cover derived from MODIS satellite images (AQUA&TERRA; MOD10A1 and MYD10A1, Version 6, (Hall and Riggs (2016), RSLE calculated based on Krajčí *et al.* (2014)
Meteorological data:					
actual climate	*T (°C) & P (mm)*	*daily sum / daily mean gridded product ca2x2km*	MeteoSwiss	1961-2018	
future scenarios	*T (°C) & P (mm)*	*daily sum / daily mean gridded product ca2x2km*	NCCS	1981-2099	45 regional models for 3 emission scenarios (see Table 2)
station data	*T (°C), P (mm), rh (-), G (-), v (m/s)*	*daily sum / daily mean*	MeteoSwiss		*13 Stations above 1500 m asl, used in Appendix B*
Glacier:					
Schweiz	*Thickness (m) & area (m2)*	*gridded product 25m x 25m*	M. Huss	1973; 2010	Area from: Müller, Caflish and Müller (1976); Maisch *et al.* (2000); Fischer *et al.* (2014); Thickness modelled by M. Huss
Europe	*Thickness (m) & area (m2)*	*mean value for every 10m elevation bands*	M. Huss	2003	Thickness modelled by M. Huss for all European glaciers. Data used for two catchments in the Rhine River basin that are located outside Switzerland.
Discharge	*Q (m3/s; mm)*	*daily/hourly/minute mean*	FOEN, Cantons, AlpiQ, OFIMA	Variable	Time series from gauging stations of 38 (nearly) undisturbed catchments

With: Regional Snow Line Elevation (RSLE), Temperature (T), Precipitation (P), Relative humidity (rh), Global radiation (G), Wind speed (v), Discharge (Q)

2.1 Delineation of the headwater catchments

The final delineation of the 190 glacierized and 5 non-glacierized headwater catchments for the river basins Rhine, Rhone, Inn and Ticino is shown in Figure 2. The choice of the catchment delineation was based on the availability of discharge time series for undisturbed catchments (as we model natural discharge) and the glacier extents. The goal was to delineate the catchments small enough to contain glacierized areas constituted of as few as possible individual glaciers and large enough to ensure the accuracy of the catchment input data. Interpolated gridded datasets such as precipitation, temperature, snow water equivalent, and remote sensed snow-covered area (SCA) need to be averaged for each catchment for modelling the discharge. Accuracy can only be ensured if a minimum amount of raster cells is used for the calculation to avoid uncertainty due to possible random errors from the interpolation methods (e.g. Rauthe *et al.*, 2013; Isotta *et al.*, 2014).

Information on the disturbance of discharge of a headwater catchment was derived from the Hydrological Atlas of Switzerland (HADES), from documentations by different water resources management operations on the construction of, e.g. dams, water diversions and returns, or other stream regulation measures, and based on internal communication with B. Schaefli (email 18.06.2018).

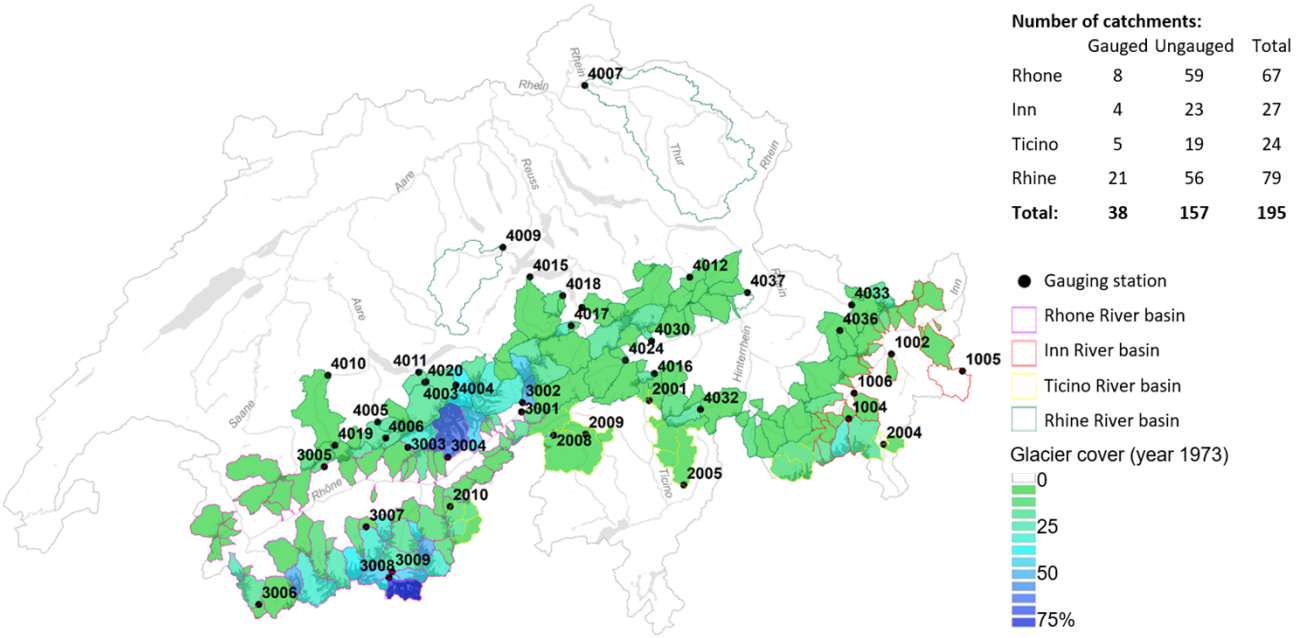

Figure 2: Delineation of all gauged headwater catchments considered in this study. The outline colors represent the River basins Rhone, Inn, Ticino and Rhine. The glacier cover (situation at the beginning of the simulation: 1973) is indicated by the background color of the catchment (green to blue). The catchment-ID of the 38 gauged catchments is labelled and corresponds to the list of all catchment characteristics of the gauged headwater catchments in Table A1 (Appendix A). The glaciers, rivers and lakes are represented in the background in light grey.

In total, 38 gauged and 157 ungauged headwater catchments were selected. Most of the gauged headwater catchments have an area between 13 and 340 km^2 with a median at 64 km^2 (only the Thur and the Kleine Emme catchments have larger areas – 1702 and 478 km^2, respectively, and were modelled for inter-model comparison with other Hydro-CH2018 project partners – see Hydro-CH2018 synthesis report: BAFU, 2021). The mean catchment elevation spreads from 768 to 3194 m asl (median: 2337 m asl), and the catchments had a glacier cover ranging from 0 to 72% (median: 3.5%). A list of all gauged headwater catchments and their characteristics can be found in Table A1 (Appendix A). The ungauged catchments have areas ranging from 5 to 277 km^2 (median: 38 km^2), mean catchment elevations comprised between 1498 and 2960 m asl (median: 2282 m asl) and glacier cover ranging from 0 to 51% (median 5.1%).

For the initial HBV-light model setup, all catchments were divided into the glacierized and non-glacierized catchment area fractions (situation at simulation start: 1973). Those areas were divided into area fractions per elevation zones (100 m for the non-glacierized part and 10 m for the glacierized part) according to the Swiss Digital Elevation Model (25x25m, DEM25) and then further differentiated within each elevation zone for three aspect classes (North-exposed: 315-45°, South-exposed: 135-225°, and indifferent: West-/East- exposed and flat areas).

2.2 Discharge measurements

For model calibration, all available discharge time series from not or only marginally disturbed (as far as documented) headwater catchments were used. Discharge time series were collected from the Federal Office for the Environment (FOEN), several cantonal water authorities (Bern, Ticino, St. Gallen), from private companies (AlpiQ, OFIMA) and from other research projects (Provided by H. Huwald, see, e.g., Simoni et al., 2011; Mutzner et al., 2015; Weijs, Mutzner and Palange, 2013). Partially, this included discharge data from hydrometric stations that do not represent the whole catchment, i.e. the gauge is situated upstream of the outlet of the modelled catchment (e.g. for catchment 3009, the gauge is located directly below the Findel glacier). In such a case, discharge data was adjusted to the catchment outlet using the specific discharge (in mm) and differences in catchment area. For two catchments (in Bleniotal and Maggiatal), only changes in the lake water level were available. In these cases, the discharge was reconstructed based on the water balance between the lake area and the water level changes.

Altogether 38 discharge time series for the time period 1973-2017 could be gathered from which five gauging stations are located in non-glacierized catchments. The gauging stations are unevenly distributed between the four river basins: 4 stations (1 non-glacierized) are located in the Inn River basin, 5 (1 non-glacierized) in the Ticino River basin, 9 in the Rhone River basin, and 21 (3 non-glacierized) in the Rhine River basin. The location of all gauging stations and their corresponding catchment delineations can be found in Figure 2, a full list of allstations and metadata is provided in Appendix A.

2.3 Meteorological datasets

2.3.1 Current climate

Meteorological data from 1970 to 2017 are needed for the model runs under current climate, on which the parameter sets are calibrated to be then used on future climate models. We use the interpolated gridded datasets RhiresD (daily precipitation sum) and TabsD (daily temperature means) provided by MeteoSwiss (stand: summer 2018). The product consists of interpolated observations on a 2x2km^2 grid with special focus on topography in the methodology. The interpolated precipitation amounts were not corrected for undercatch of the measurement stations. More information on the products and the interpolation methods can be taken from the product descriptions (Frei and Schär, 1998; Schwarb, 2000; Frei, 2014; Isotta *et al.*, 2014). For each catchment, we calculated the mean precipitation sum (P) and mean temperature (T) on a daily basis as the weighted mean of all entire and partial grid cells within the catchment boundaries.

2.3.2 Future climate scenarios

For hydrological modelling under future climate conditions, we use the CH2018 Climate Change Scenarios from the National Center for Climate Services (NCCS; CH2018 project Team, 2018). Daily temperature means and precipitation sums from 45 climate models for three emission scenarios (best case: RCP2.6, RCP 4.5 and worst case: RCP 8.5) were provided by MeteoSwiss as a gridded product on the same grid and projection as the RhiresD and TabsD datasets. The time series are available for the period 1981-2099. A list of all emission scenarios and corresponding climate models is given in Table 2.

Table 2: Climate scenarios and models used for modelling of future discharge.

Global model	Run	Regional model	RCP		
			8.5	4.5	2.6
ICHEC-EC-EARTH	r1i1p1	KNMI-RACM022E	x	x	
	r3i1p1	DMI-HIRHAM5	x	x	x
	r12i1p1	CLMcom-CCLM4-8-17	x	x	
		CLMcom-CCLM5-0-6	x		
		SMHI-RCA4	x	x	x
MOHC-HadGEM2-ES	r1i1p1	CLMcom-CCLM4-8-17	x	x	
		CLMcom-CCLM5-0-6	x		
		ICTP-RegCM4-3	x		
		KNMI-RACM022E	x	x	x
		SMHI-RCA4	x	x	x
MPI-M-MPI-ESM-LR	r1i1p1	CLMcom-CCLM4-8-17	x	x	
		CLMcom-CCLM5-0-6	x		
		SMHI-RCA4	x	x	x
	r2i1p1	MPI-CSC-REM02009	x	x	x
MIROC-MIROC5	r1i1p1	CLMcom-CCLM5-0-6	x		
		SMHI-RCA4	x	x	x
CCCma-CanESM2	r1i1p1	SMHI-RCA4	x	x	
CSIRO-QCCCE-CSIRO-Mk3-6-0	r1i1p1	SMHI-RCA4	x	x	
IPSL-IPSL-CM5A-MR	r1i1p1	SMHI-RCA4	x	x	
NCC-NorESM1-M	r1i1p1	SMHI-RCA4	x	x	x
NOA-GFDL-GFDL-ESM2M	r1i1p1	SMHI-RCA4	x	x	

As our model simulations start in 1973 (due to data availability on glacier cover) with warming up from 1970, precipitation and temperature were consequently calculated for all 195 gauged and ungauged headwater catchments for the time period 1970-1980 from the RhiresD and TabsD gridded products and from 1981-2099 for the 45 climate models to obtain a time series of the right length. These time series are used for model runs of future discharge (Section 5), the analysis of the results, however, was only performed on the 1981-2099 model outputs for consistency.

2.3.3 Correction of precipitation data

The gridded precipitation products (RhiresD and Climate change scenarios from NCCS) are uncorrected for undercatch of the measurement stations, which can be especially large, the higher the elevation. As a result, the annual precipitation sum calculated directly from RhiresD was for most of the gauged catchments (38) underestimated compared to the observed annual discharge. To correct the precipitation mean of all 195 headwater catchments (gauged and ungauged), the mean annual precipitation sum for 1961-1990 was calculated for all headwater catchments a) from the RhiresD gridded dataset ($P_{RhiresD,1961-1990}$), and b) using the precipitation values given in HADES (Table 6.3) and derived from the water balance ($P_{HADES,1961-1990}$). $P_{HADES,1961-1990}$ was scaled to the delineation of the 195 headwater catchments using a weighted mean based on the sub-catchment areas. As a different DEM was used for each of the datasets, a precipitation-elevation gradient was calculated based on the RhiresD product for each catchment (see Section 2.3.4), and the precipitation mean was then corrected for each product for the mean catchment elevation. A correction factor was finally calculated for each headwater catchment as the fraction between $P_{HADES,1961-1990}$ and $P_{RhiresD,1961-1990}$ and applied to all precipitation time series used in the project (RhiresD for current climate and CH2018 for future scenarios). It was assumed that the correction factor is constant over time. Since a challenge in hydrological modelling is to cope with situations where the total amount of precipitation is smaller than the total amount of discharge, a correction was only applied if the correction factor was >1. In total, 78% of the headwater catchments needed a correction. On average, the correction factor was 1.13, with a maximum value of 1.79. The spatial distribution of the correction factors is shown in Figure 3.

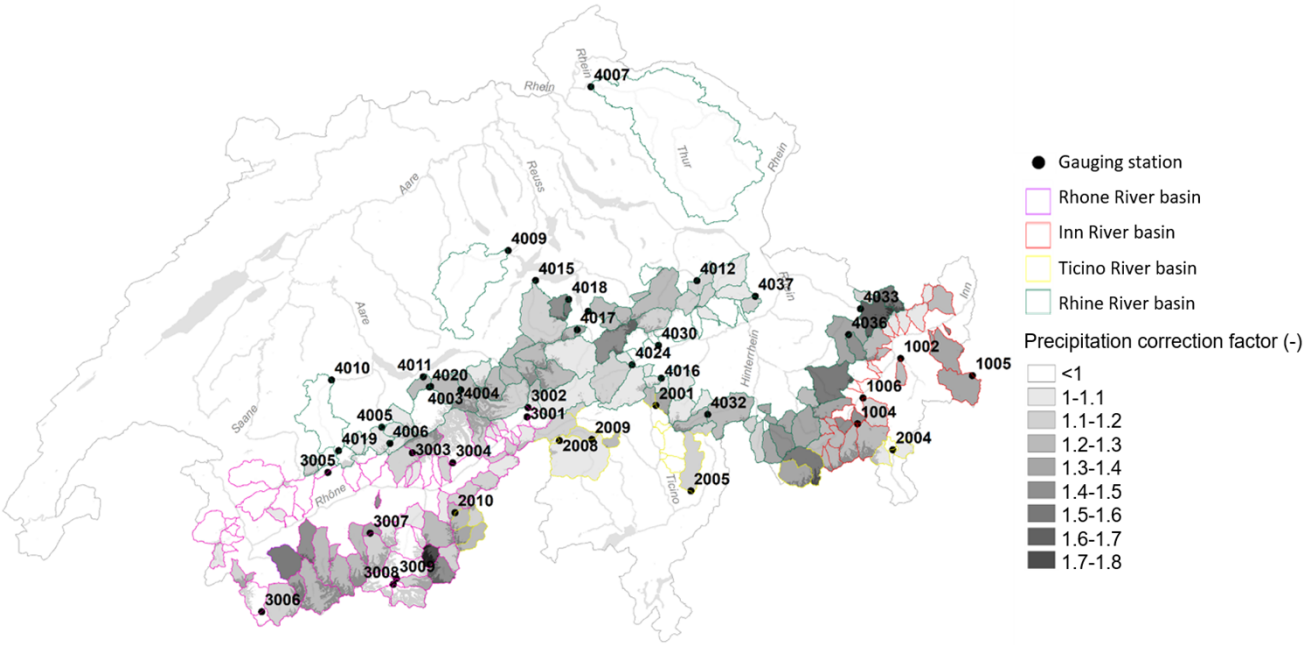

Figure 3: Spatial distribution of the precipitation correction factors over the 195 headwater catchments. The outline colors represent the River basins Rhone, Inn, Ticino and Rhine. The value of the correction factor is indicated by the background color of the catchments (white to dark grey). The catchment-ID of the 38 gauged catchments is labelled and corresponds to the list in Table A1 (Appendix A). The glacier cover, rivers and lakes are visible in the background in light grey.

2.3.4 Precipitation and temperature gradients

Precipitation and temperature gradients (dT and dP) are needed as input data for the HBV-light model to correct the meteorological data for the different elevation zones in the catchments as the semi-distributed model HBV-light is based on hydrological response units. The gradientswere calculated based on the daily values of the interpolated meteorological products and on the given DEM of the products. A linear relationship was assumed between the daily P or T values and the elevation of all grid cells in a headwater catchment.

As precipitation gradients have large uncertainties, dP was assumed to be constant over time and was calculated for each headwater catchment based on the RhiresD product (Section 2.3.1) for the current climate and the CH2018 product (Section 2.3.2) for future climate scenarios as the mean daily value over the entire period (1973-2017 and 1981-2099, respectively). For the temperature gradient, time series of daily dT values calculated based on the respective temperature products for current and future climates were used.

2.3.5 Potential evapotranspiration (PET)

Daily potential evapotranspiration (PET) is needed as input data in the HBV-light model and was calculated for all 195 gauged and ungauged headwater catchments using the temperature datasets described in Sections 2.3.1 and 2.3.2 and the Hamon equation (Hamon, 1963; Eq. 1) to be in adequation with the other Hydro-CH2018 project partners. To ensure that the Hamon equation was adequate to be used for our modelling purposes, we compared several equations to calculate potential evapotranspiration. Overall, Hamon performed as well as the other equations (see Appendix B).

$$PET = \left(\frac{N}{12}\right)^2 \cdot e^{T/16} \qquad (1)$$

With N: maximum possible hours of daylight on Julian day (h), T: mean daily temperature (°C).

2.4 Snowpack

2.4.1 Snow water equivalent

Mean daily snow water equivalent (SWE) is needed for all 195 catchments for the snow calibration of the HBV-light model. The WSL Institute for Snow and Avalanche Research (SLF) provided a gridded product of interpolated daily SWE values for entire Switzerland on a 1x1km grid for the period 1990-2017. This product was derived from the interpolation of measured snow heights (up to 344 stations) coupled to a physically-based snow model for the estimation of SWE (Jonas, Marty and Magnusson, 2009). The spatial distribution of the SWE was assessed with regional patterns of SWE with elevation. The effect of topography and land cover was conceptually assessed within each grid cell. More details on this product can be found in Freudiger *et al.* (2016). As the SWE values are uncertain at very high elevation due to the lack of observations, the mean daily SWE value was calculated for each headwater catchment as the weighted mean of all grid cells up to 2500 m asl elevation.

2.4.2 Snow cover

Additionally to the mean SWE values (providing information on snow amounts), a time series of regional mean snow line elevation (RSLE) for each headwater catchment was used for model calibration to provide information on the extent of the snow cover. RSLE represents the mean elevation above which the area is mainly snow-covered and under which it is mainly snow-free. The RSLE values were estimated from the snow products of the MODIS satellite images (MOD10A1 and MYD10A1, Version 6, Hall and Riggs, 2016; 500 m resolution) and following the RSLE-calculation method of Krajčí *et al.* (2014) as described in Hrachowitz, Fugger and Schulz (2020). In this method, RSLE is determined as the average snow line elevation from partially cloud-obscured raster imagery for a given region (min. 100 km^2). The main advantage of RSLE compared to direct use of Snow covered area from satellite products, is that RSLE can be also derived on partly cloud covered days.

A time series of RSLE was derived by S. Fugger for the aim of our project for the period 24.02.2000-23.09.2018 and for the entire catchment as well as for three aspect classes (North, South, indifferent: East, West or flat) for the 195 headwater catchments. RSLE values were calculated for clusters of headwater catchments (always within the same river basin) to ensure that a minimum size of 100 km^2 was reached. The RSLE values were derived for the non-glacierized part of the catchments only (glacier cover situation in 2003 taken as constant over the entire period), as it is difficult to distinguish between snow and ice in MODIS images. RSLE values were

computed for the three aspect classes only for aspect zones with an area >37.5 km^2 (150 pixels), to capture differences in snow line elevation caused by different accumulation and melt conditions. All headwater located within a cluster received the RSLE derived for the given cluster.

The accuracy of the calculated RSLE values was assessed on each time steps based on the cloud cover and the non-ambigousness of the snow detection for the given day. In HBV-light, this uncertainty information is then used to weight the information of the RSLE for a given day for the calibration of the snow cover. The combination of the SCA derived from RSLE with the SWE information (Section 2.4.1) gives us two independent sources of information to assess for the spatial distribution of the snow as well as the snow amounts during the calibration processes in HBV-light.

2.5 Glacier observations

Besides the general catchment model setup (see Section 2.1), the initial glacier profile had to be defined for transient simulation of the glacier area (see also Section 3.3). The glacier area and water equivalent were estimated for all headwater catchments and for 10 m elevation bands for the year 1973 using the Swiss-wide thickness data provided by M. Huss (see Table 1) and using an ice density of 900 kg/m^3. This glacier profile represents the glacier cover at the start of the simulation in HBV-light (1973).

For the calibration of glacier volume change, we estimated the total change in water equivalent for the glacier area of each headwater catchment between the years 1973 and 2010 using the thickness data provided by M. Huss for those two periods.

2.6 Sources of uncertainties

Hydrological modelling is subject to uncertainties, especially when modelling under future climate scenarios. Besides the fact that hydrological models are a simplification of reality, the source of uncertainties differs and might be difficult to assess exactly. Multi-criteria calibration ensures that all processes are simulated as exact as possible compared to observations, but its robustness largely depends on the quality of the observations. To minimize this uncertainty source, the accuracy of the datasets was, when identifiable, taken into account in the weighting and choice of the objective functions (e.g. for discharge, see Section 4) as well as in the time series themselves when uncertainty information was available (as for RSLE, Section 2.4.2).

One large source of uncertainty is the regionalization approach (Section 4.2) for headwater catchments with no discharge observations. This uncertainty was minimized by the use of an ensemble mean for the simulated discharge out based on five transferred parameter sets (see also Appendix C). Furthermore, a test of the regionalization approach on gauged catchments, showed that the discharges time series obtained by regionalization were comparable to the observed data (see example in Appendix C).

One other source of uncertainty when modelling future discharge are the climate models themselves, and the uncertainty increases with time. The use of a large amount of climate models allows covering a large range of uncertainty. A full assessment of the uncertainty of the climate models can be found in CH2018 (2018). For clarity reasons, we only show the median of all climate models used in the data analysis (Section 5), but the results between the different climate models show a large variability that needs to be taken into account for when interpreting the results (i.e., one has to be aware of the range of simulations for the future). Due to the different sources of uncertainties, the presented results are an estimation of the behaviour of the contributions to the total discharge of rain, snow and glacier melt for near and far future and are not meant to be used as absolute values.

3. HBV-light

The hydrological model has been developed in the 1970s in Sweden (Bergström, 1976) and is nowadays widely used worldwide under different versions for runoff simulation. The use of hydrological models for determining discharge components in glacierized catchments, their dynamics and their long-term changes for past, present and future climate is necessary. This is especially true for ungauged catchments or for gauged catchments with

short time observations. The main challenge of the hydrological modelling of discharge components in glacierized catchments is to represent the different hydrological processes in the glacierized and non-glacierized part of the catchments as good as possible to minimize the uncertainty of the simulated discharge components. In this study, we use a version of the semi-distributed bucket-type hydrological model HBV-light (Seibert and Vis, 2012) that was specially customized during the ASG1-project (Stahl et al., 2016) to (1) track the discharge components rain, snow and glacier melt in total discharge, (2) assess for snow redistribution to avoid snow towers in high elevation zones for long-term modelling of the snow cover, and (3) to assess for the transient changes of glacier area and volume. These main model features are shortly explained in the next sub-sections. More detailed information can be found in Stahl *et al*. (2016) and Seibert *et al.* (2017).

3.1 Tracking the discharge components

All water within the model is labelled as originating from rain, snow or glacier melt, and traced throughout the model. The (liquid) water content of a snowpack can be a mixture of water originating from snow and rain, depending on whether it results from snowmelt or from rain on top of the snowpack. In case a snowpack is located on a glacier, the outflow from the snowpack will enter the (liquid) water content of a glacier, which can therefore be a mixture of water originating from rain, snow and/or glacier melt. In glacierized areas outflow from the glacier routine is going directly to the routing routine to represent overland flow. In non-glacerized areas water is infiltrating into the soil. The soil box offers two options: 'perfect mixing' and 'bypass'. In case of perfect mixing, water entering the soil box is fully mixed with the water already present before recharge is extracted. This causes a delay and results in, for example, an extension of the period in spring/summer where a snow component is present in the discharge. In case of the bypass option, the composition of recharge is identical to the composition of the water infiltrating into the soil, i.e. snow and glacier meltwater are directly contributing to the discharge.

3.2 Snow model

In HBV-light, snow water equivalent is calculated with the degree-day approach and melt is produced at different speeds depending on the aspect of the given elevation zone (see Konz and Seibert, 2010). The degree-day factor varies within a year following a sinus function, as suggested by Stahl *et al.* (2008). Sublimation of the snow cover is represented by a calibrated parameter. Snow redistribution by wind and avalanches may play an important role in discharge modelling, and taking these processes into account may avoid unrealistic snow towers at high elevations for long-term modelling (e.g. Freudiger *et al.*, 2017). A conceptual snow redistribution routine was therefore included in HBV-light to better represent the spatial distribution of snow. Above a specified elevation (here: 2600 m asl), if snow accumulation is larger than a fixed SWE value (here 500 mm), the surplus amount of snow is then redistributed over the entire glacier area (as it was at the beginning of the simulation, here:1973) and the non-glacierized area between two threshold elevations (here: 1900 to 2600 m asl) and weighted equally between the receiver areas (see Stahl et al. (2016) for further details). We assume that glacier areas represent preferred deposition areas for precipitation due to topography (e.g. Carrivick and Brewer, 2004; Huss and Fischer, 2016) and that this characteristic will not change if the glacier has completely retreated.

3.3 Glacier model

Ice melt is computed using the degree-day approach and added to the water content of the glacier. Outflow from the glacier is based on the water content of the glacier and the snow water equivalent on the glacier as defined in Stahl et al. (2008; equations 2 and 3). Especially for long-term modelling of glacierized catchments, it is important that models are able to catch the spatial and temporal changes of glacier cover in a transient way. To this aim, a new glacier routine was implemented in HBV-light (Seibert et *al*., 2018), whereby the glacier extent is updated every year to keep area and mass balance consistent. In order to do so, the glacier profile at the beginning of the simulation (area and thickness for 10 m elevation bands) needs to be provided by the user. The Δh-parameterization method as described in Huss *et al.* (2010) is then applied to establish a relationship between changes in glacier mass balance and area changes of the glacier. At the end of each hydrological year the areal distribution of the glacier that corresponds to the simulated mass balance at that moment in time is then applied to the glacier.

4. Model calibration

Multi-criteria calibration is essential to ensure that all hydrological processes in the glacierized and non-glacierized parts of the catchments are well-represented by the model (e.g., Seibert, 2000; Stahl et *al*., 2008; Konz and Seibert, 2010, Finger et *al*., 2015). The 195 mostly glacierized headwater catchments of this project were therefore calibrated on discharge observations (when available), as well as on information on snow and glacier cover that was derived from several available datasets (see Section 2).

This project aims at the best possible simulation of the discharge over a long period (future climate) in regions, where data are rather scarce. Additionally, the time series used for calibration (discharge, SWE, RSLE and glacier changes) are of different length and timing for each headwater catchment. Therefore, we decided to incorporate all available observational information over the whole period 31.10.1973 to 31.12.2017 for the multi-criteria calibration of the HBV-light model. We used three years (1970-1973) for model warm-up.

For the calibration of all gauged and ungauged headwater catchments, a genetic parameter optimization algorithm was applied using the GAP-tool implemented in HBV-light (see Seibert, 2000) evaluated with weighted objective functions. The calibration procedures, the weights and the choice of the goodness of fit measures used for discharge, snow and glacier cover are based on previous analyses from the ASG1-project (Stahl *et al.*, 2016). In these analyses, the weight of each goodness of fit measure has been defined in a qualitative assessment through an iterative process, including several test simulations with different calibration settings and weights. In the GAP-algorithm, parameter sets are genetically created over more than 3500 runs and 1 calibration.

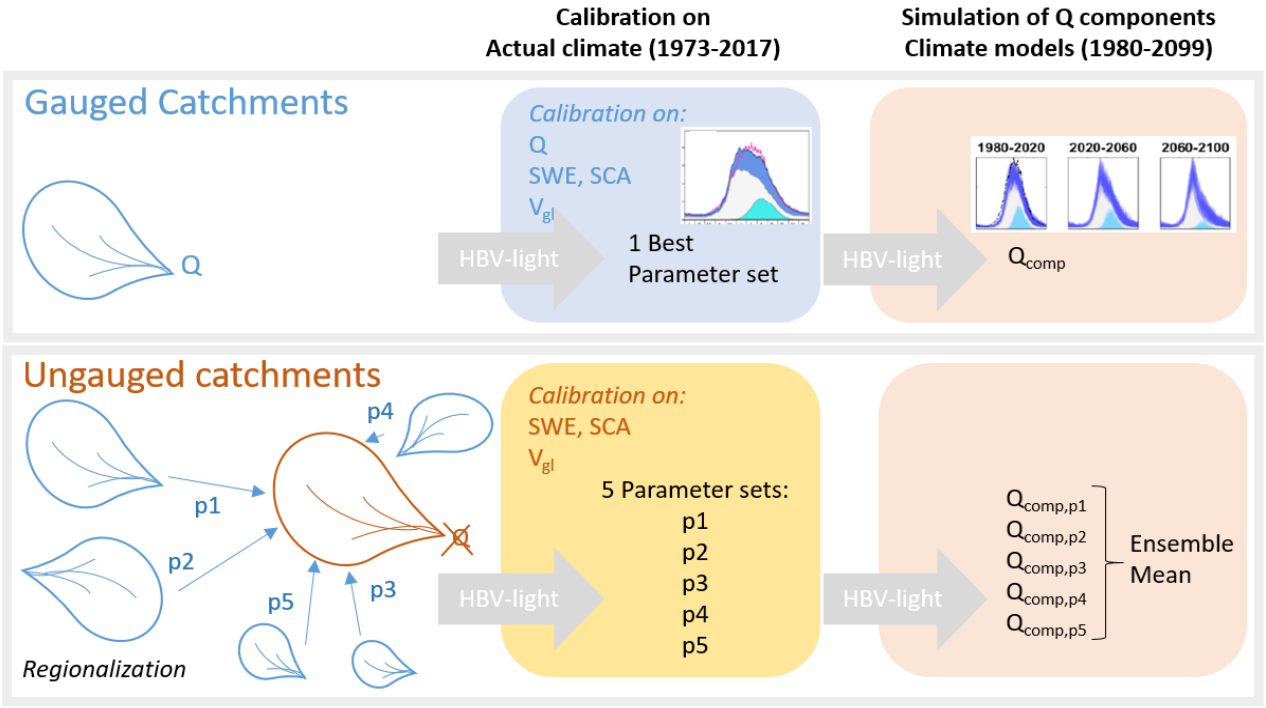

Q: Discharge, Q_{comp}: Discharge components, SWE: Snow water equivalent, SCA: Snow covered area, V_{gl}: Glacier volume

Figure 4: Schematic representation of the calibration procedures used (1) for the 38 headwater catchments with observed discharge data available, and (2) for the 157 ungauged headwater catchments. With Q: the discharge, Q_{comp}: the discharge components, SWE: the snow water equivalent, SCA: the snow-covered area, V_{gl}: the changes in glacier volume, and p1-p5: the calibrated parameter sets.

The calibration procedures for the gauged and ungauged headwater catchments are schematically represented in Figure 4. First, all 38 gauged catchments were calibrated with a given weight on discharge (50%), snow (RSLE and SWE; 30%) and glacier volume (20%). Three different objective functions were used for discharge calibration in order to account for seasonality – high flow in summer assessed with the seasonal Nash-Sutcliffe Efficiency for the period June 1st to September 30th (weighted 15%) and low flow in winter assessed with the

logarithmic Nash-Sutcliff Efficiency (weighted 15%) – as well as the volume assessed with the Lindström Efficiency (weighted 20%). For 7 catchments, the quality of the observed discharge could not be fully ensured. In such cases, discharge was calibrated with the Spearman Rank goodness of fit only. Details on the calibration methods for gauged catchments can be found in Appendix C.1. After calibration, the best parameter set was taken to simulate discharge for present and future climate.

Second, a parameter transfer approach was used to regionalize the best parameter sets obtained for the 38 gauged catchments to the 157 ungauged catchments. Each ungauged catchment received the calibrated model parameters from five gauged donor catchments. To find these donor catchments, all catchments were compared based on their characteristics (distance from each other, catchment area, slope, aspect and elevation, glacier cover, meteorological characteristics, region and groundwater type). Once the five gauged donor catchments were identified, the five parameter sets were transferred to the given ungauged acceptor catchment and were re-calibrated based on snow (RSLE and SWE; 60%) and glacier volume (40%) using the same algorithm as for the gauged catchments. Details on the regionalization approach and the calibration for ungauged catchments can be found in Appendix C.2. These five parameter sets were then used to simulate discharge for present and future climate. The results for the ungauged catchments presented in Section 4 and 5 represent the ensemble mean of the five simulated time series.

4.1 Results of the multi-criteria calibration of the gauged catchments

In Figure 5, the goodness of fit measures are presented for all 38 gauged headwater catchments. Due to the small amount of available glacier observations, the model is calibrated only on the glacier volume in 1973 and 2010, meaning two data points. Therefore, the objective function is always very close to 1. The discharge objective function with the largest spread is the Seasonal Nash-Sutcliffe Efficiency for flows from Jun-1 to Sep-30 (R_{Q3}), which is largely influenced by snowmelt. As snow observations are nowadays still difficult to obtain in high elevated alpine catchments, these results are not surprising.

As expected, some differences among the catchments and among the different objective functions may be noted. But, overall, the simulation results are in a reasonable range. The weighted objective function R is comprised between 0.68 and 0.94 (median: 0.87) for all 38 gauged catchments. It can consequently be stated that the discharge, snowpack and glacier changes could be adequately represented by the described version of the HBV-light model, as required for the aims of this project.

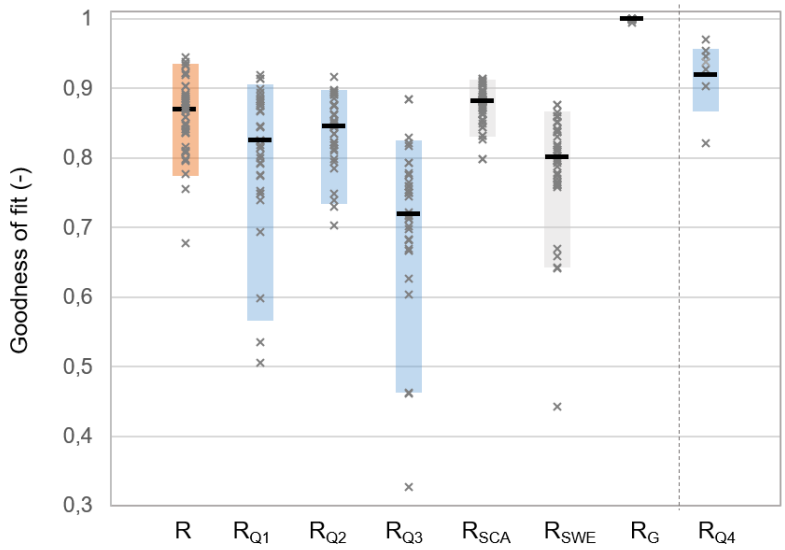

Figure 5: Goodness of fit values obtained after model calibration for the 38 gauged catchments. The boxes show the 5th and 95th percentile, the bold line is the median, and the crosses are the single values. All efficiency measures from Eq. 2-4 are shown (see Appendix C.1). Orange: weighted objective function (R), blue: streamflow (R_{Q1}: Lindstrom Measure, R_{Q2}: Nash-Sutcliff efficiency of logarithmic flow, R_{Q3}: Seasonal Nash-Sutcliffe Efficiency, R_{Q4}: Spearman Rank – used for 7 catchments), grey: Snow (R_{SCA}: Root mean square error, R_{SWE}: Mean absolute normalized error) and glacier (R_G: Absolute mean relative error).

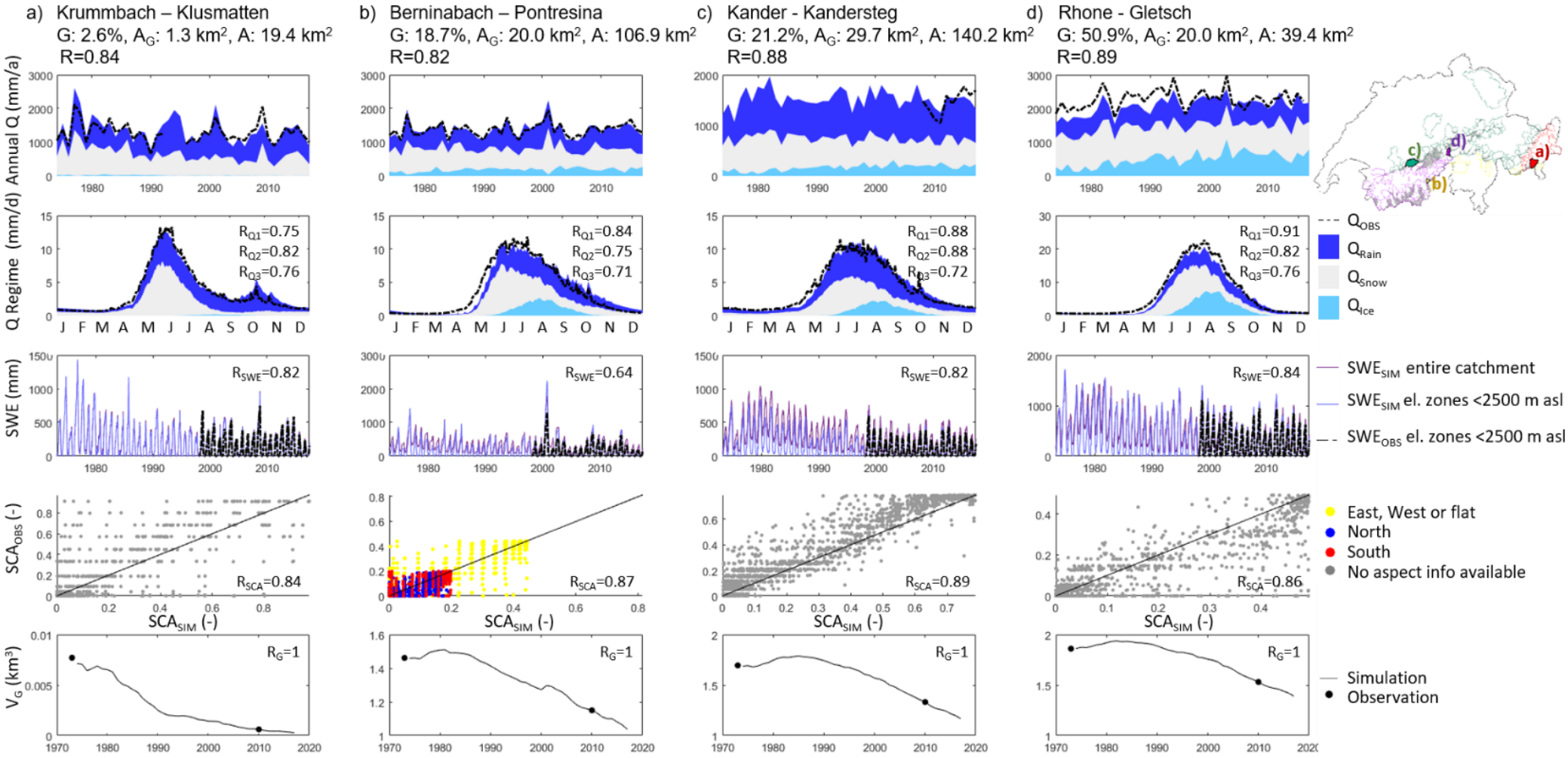

Figure 6: Example of calibration results for four catchments with increasing glacier cover (from left to right). With G: glacier cover, A_G: glacier area, A: catchment area, Q_i: discharge components, SWE: snow water equivalent, SCA: snow covered area, V_G: glacier volume. The objective functions are given as indicated in Appendix C.1 (R_{Q1}: Lindstrom Measure, R_{Q2}: Nash-Sutcliff efficiency of logarithmic flow, R_{Q3}: Seasonal Nash-Sutcliffe Efficiency, R_{Q4}: Spearman Rank – used for 7 catchments, R_{SCA}: Root mean square error, R_{SWE}: Mean absolute normalized error and R_G: Absolute mean relative error)

Calibration results are shown in Figure 6a-d for four selected headwater catchments with different glacier cover spread over the four River basins Inn, Ticino, Rhine and Rhone. The observations and the goodness of fit values are given in the corresponding sub-figures. The discharge regimes in Figures 6b to 6d illustrate how the discharge is slightly underestimated during the snowmelt period in spring as expected from R_{Q3} in Figure 5. Overall, the snow water equivalent is well assessed for all four catchments. Some larger snow amounts are accumulated in the 1980s for the mean catchment's SWE at the highly glacierized catchments Kandersteg (Figure 6c) and Gletsch (Figure 6d), but snow towers could be avoided thanks to the snow redistribution routine (see Section 3.2). Only the catchment of the Berninabach had aspect information for the snow-covered area derived from the RSLE. For all four catchments, the glacier volume meets well the glacier observations of 1973 and 2010.

4.2 Calibration results for the ungauged headwater catchments

After calibration of the 157 ungauged catchments with the parameter sets of five donor catchments, the spread between the five simulated discharge time series was small for more than 85% of the catchments. In 15% of the catchments, however, one of the five parameter sets would react completely differently than the other ones. To illustrate this issue, Figure 9 shows calibration results for two ungauged catchments. In Figure 9a, the spread between the five parameter sets is relatively small and transferring the "best" parameter set only (from the most similar donor catchment, Rank=1) would have been sufficient. In Figure 9b, in contrary, one parameter set, which, in this case, happens to be the "best" parameter set (rank=1), is leading to completely different results than the other four parameter sets. However, this parameter set has only little influence on the ensemble mean of the model outputs with the five parameter sets. This last example shows the importance of using an ensemble mean of the model outputs of several parameter sets instead of using only the best parameter set for the calibration of the ungauged catchments. The number of five parameter sets was chosen as it is small enough to ensure suitable computational time for the calibration and large enough to minimize the effect of potential outliers by using the ensemble mean of the modelled discharge components.

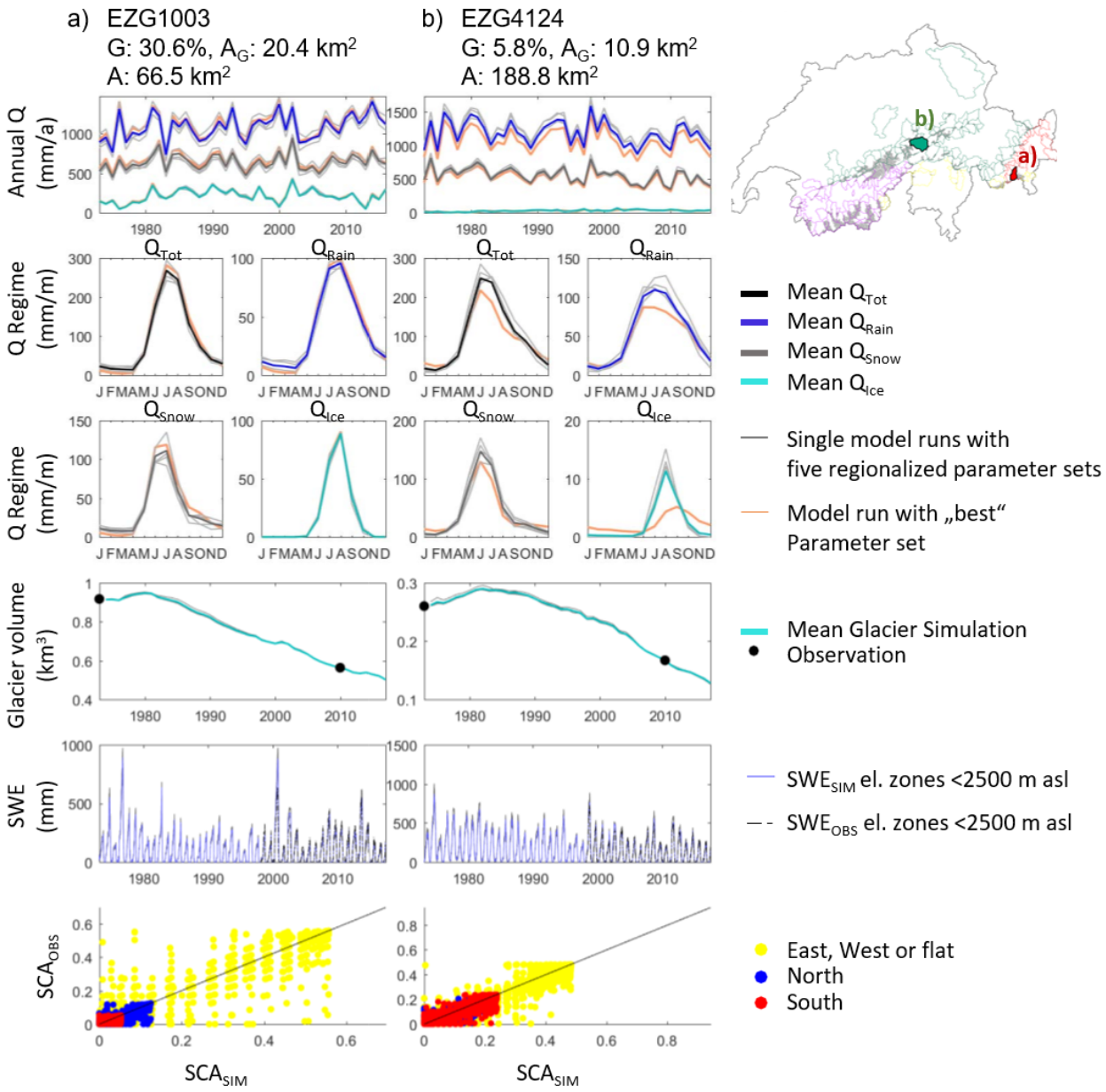

Figure 7: Calibration results for two selected ungauged catchments (nr 1003 in the Inn River basin and nr 4124 in the Rhine River basin). a: good agreement between the five transferred parameter sets and b: low agreement for the best parameter set.

Take home message from the calibration

- The multi-criteria calibration on independent observation data such as discharge, regional snow line, snow water equivalent time series and glacier volumes enables to ensure that all aspect of the hydrographs are modelled accurately.
- The regionalization of the parameters responsible for discharge from 5 gauged donor catchments to the ungauged acceptor catchments allows us to assess the discharge components for all 157 ungauged catchments. The recalibration of the parameters responsible for snow and glacier melt ensured that all processes were represented best.

5. Simulation of future discharge components

Total discharge (Q_{tot}) and its discharge components from rain (Q_{Rain}), snow (Q_{Snow}), and ice melt (Q_{Ice}) were modelled with HBV-light for the emission scenarios RCP 2.6, RCP 4.5, and RCP 8.5 and a total of 45 climate models using the calibrated parameter sets obtained in Section 4. We only show the results for the best-case and worst-case scenarios RCP 2.6 and RCP 8.5. Usually, we show the median of all climate change models for one emission scenario (8 model runs for RCP 2.6 and 21 for RCP 8.5). The aim was to assess how climate change may impact the different discharge components to understand future changes in total discharge better. In this section, we analyze the changes of the simulated discharge components for two 30-yr periods centred at 2060 and 2085 (2045-2074 and 2070-2099) compared to the 30-yr reference period 1981-2010. One has to note that the precipitation and temperature datasets of the current climate (RhiresD and TabsD) were only used to calibrate the hydrological model (see Section 2 and Section 4). For consistency in the comparisons of the different periods, we only use the simulation results of the future climate models (available for 1981-2099) for the assessment of the long-term changes in discharge components. The reference period refers, therefore, to the given period in the 45 future climate models.

5.1 Changes in discharge components

Figure 10a shows the spatial distribution of the mean annual contribution of rain, snow and ice melt during the reference period ($Q_{comp,ref}/Q_{tot,ref}$ x 100). Q_{Ice} is, as expected, the smallest contribution to discharge for most of the catchments with an average of ca. 7% of total discharge. However, in some catchments of the Rhone River basin, ice melt contribution can reach up to 57%. Q_{Snow} plays an important role for all alpine headwater catchments with large regional differences, with contributions to discharge ranging from 12% to 58% (mean: 35%). Q_{Rain} is for most catchments the largest contribution to total discharge with contributions ranging from 23% to 88% (mean: 57%). However, a few high elevated catchments of the Rhone and Rhine River basins have overall a higher contribution from snow and ice melt than rainfall.

In Figure 10b, the spatial distribution of changes in Q_{tot}, Q_{Rain}, Q_{Snow}, and Q_{Ice} is presented for the emission scenarios RCP 2.6 and RCP 8.5 as the average for two 30-yr periods centred at 2060 and 2085 and compared to their own contribution during the reference period ($Q_{i,future}/Q_{i,ref}$ x 100). For emission scenario RCP 8.5, total discharge is expected to slightly decrease for most of the catchments around 2085 compared to the reference period with values ranging between -39% and +26% units (mean: -9%). For 17% of the catchments, the change in Q_{tot} is comprised between -5 and +5% units, and only 3 catchments are expected to have changes larger than +5% units (amongst others the catchment of the Aletsch glacier). The largest decreases are expected in the North/West of the Rhone River basin (Figure 10b). For best-case scenario RCP 2.6, Q_{tot} is expected to only slightly increase in the Eastern half of the Swiss Alps (mostly Ticino, Inn and part of the Rhine River basins) and slightly decrease in the Western half of the Swiss Alps with values ranging from -25% to +12% units (mean: +0.5%) for all catchments.

Even if changes in Q_{tot} are relatively small for both emission scenarios, the contributions of the different discharge components might still be impacted by climate change, which may induce large changes in the seasonality of the discharge regime (see Section 5.2) and have important consequences for future water resources management. Q_{Rain} is expected to increase for all catchments and for both emission scenarios with a slightly larger increase for RCP 8.5. This increase can be related to an overall increase in liquid precipitation, especially in winter (CH2018, 2018). Q_{Ice} is expected to have the largest negative changes around 2085, with its contribution decreasing on average by -92% units (ranging from -13% to -100%) and a median at -98% units for RCP 8.5 and only slightly smaller for RCP 2.6. These results were expected as most of Swiss glaciers might have retreated entirely until the end of the century and are expected to lose up to 80% +/- 15% of their total volume (e.g. Huss et *al.*, 2017). The small differences between both emission scenarios indicate that glaciers react with delay to climate change. Even the best-case scenario would not allow to slow down the glacier retreat significantly (e.g. Zekollari et *al.*, 2020). On average, ice melt contribution to total discharge around 2085 ($Q_{ice,2085}/Q_{tot,2085}$ x 100) is expected to be ca. 1.4% for all glacierized catchments under RCP 8.5 and ca. 2% under RCP 2.6. However, some regional differences will be observed and some large glaciers, mostly in the Rhone River basins, will continue to significantly contribute to discharge at the end of the century. Independently of

the emission scenario, only 7 out of the 190 glacierized headwater catchments will have Q_{Ice} contribution to total discharge remaining larger than 10% at the end of the century (largest values < 30% for the catchments of the Aletsch and Gorner glaciers – ID 3004 and 3008). Only four catchments still have a positive change in Q_{Ice} around 2060 in RCP 8.5. Q_{Snow} has the most interesting regional patterns and the largest differences between both emission scenarios with values ranging from -42% to +29% units (mean: -19%) for RCP 8.5 and ranging from -22% to +26% units (mean: -6%) for RCP 2.6 at the end of the century. Even if in most catchments the changes in Q_{Snow} are decreasing, Q_{Snow} still has positive changes around 2060 in 8 catchments in RCP 8.5, but only in 4 around 2085. These positive changes concern mostly the high elevated catchments in the Rhone and Rhine River basins.

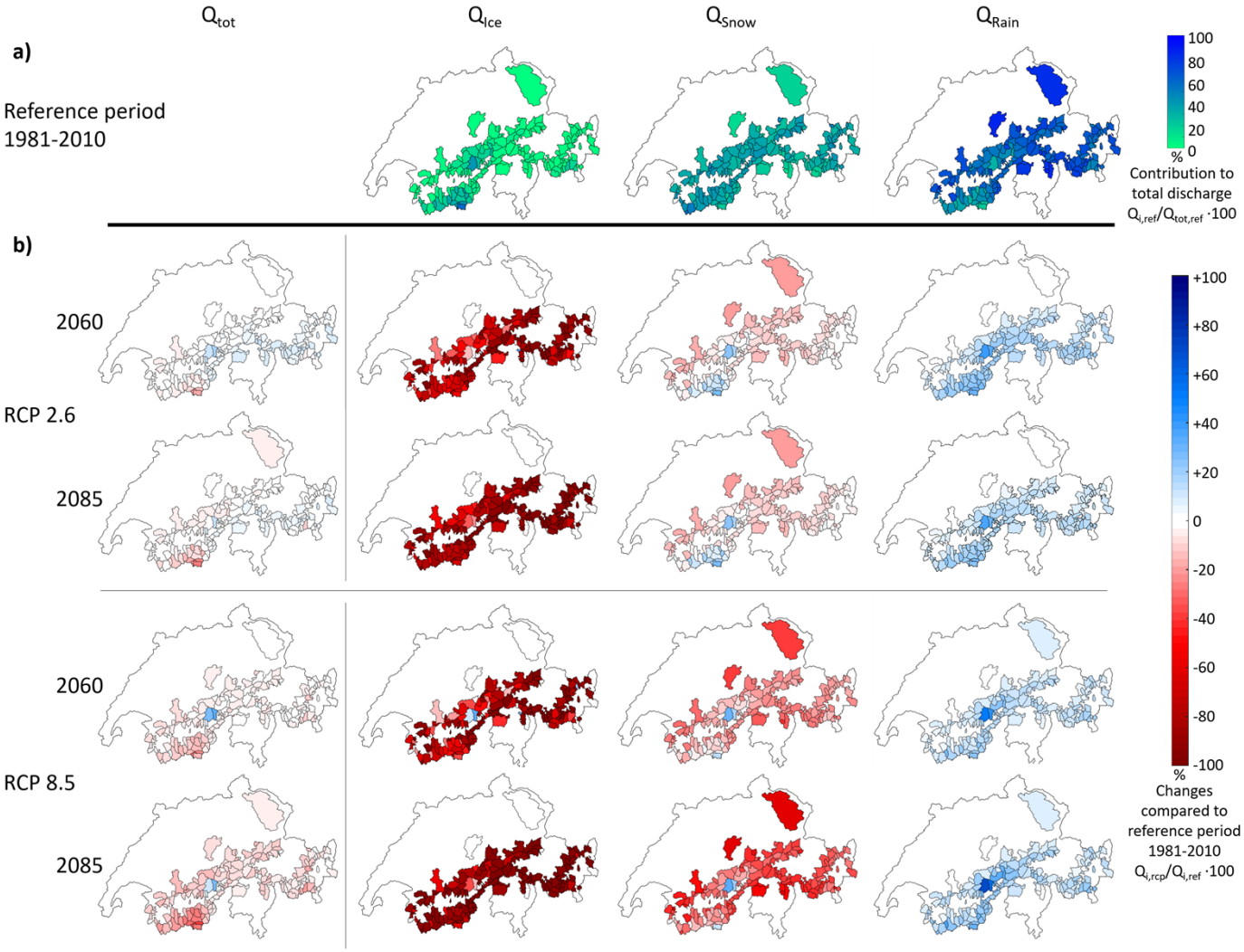

Figure 8 Spatial representation of the mean changes in the annual total discharge (Q_{tot}) and in the annual contribution of rain (Q_{Rain}), snow (Q_{Snow}) and ice melt (Q_{Ice}) for two 30 yr-periods centred at 2060 and 2085 for the emissions scenarios RCP 2.6 and RCP 8.5 compared to the contribution during the reference period ($Q_{i,rcp}/Q_{i,ref}$ x 100). Presented is the median of all climate change models for the given emission scenarios (9 for RCP 2.6 and 21 for RCP 8.5) and for the 195 headwater catchments. The upper line of the Figure (a) shows the mean contribution to total discharge during the reference period ($Q_{i,ref}/Q_{tot,ref}$ x 100).

In Figure 11a-b, the mean changes in discharge components are related to the mean catchment elevation. Changes in Q_{Snow} and Q_{Rain} seem to be more positive, the higher the catchment in both emission scenarios. Changes in Q_{Ice} are independent of the mean catchment elevation and might be influenced by other factors such as glacier volume at the beginning of the simulation, mean glacier elevation, slope and aspect (e.g. Huss and Fischer, 2016; Zekollari et *al.*, 2020). Interesting is the shift in the change of Q_{tot} for mean elevations > ca. 2500 m asl from rather no trend to a rather negative trend dependent on the mean catchment elevation. Above 2500 m asl, glacier coverage is for all catchments larger than 17% (Figure 11c). At the end of the century, the glacier melt contribution to the total discharge of most of the catchments with glacier coverage >17% is larger than 5% (Figure 11d). Consequently, the rather negative trend of Q_{tot} observed for high elevated catchments can be explained by large losses in glacier melt contribution in high elevated catchments, where the glacier cover is large enough to significantly influence the total discharge until the end of the century. The differences between RCP 2.6 and RCP 8.5 in the changes of the discharge components in Figure 11 support the conclusion from Figure 10 that Q_{Snow} might still play an important role for future discharge compared to Q_{Ice} and experience the largest difference between RCP 2.6 and RCP 8.5.

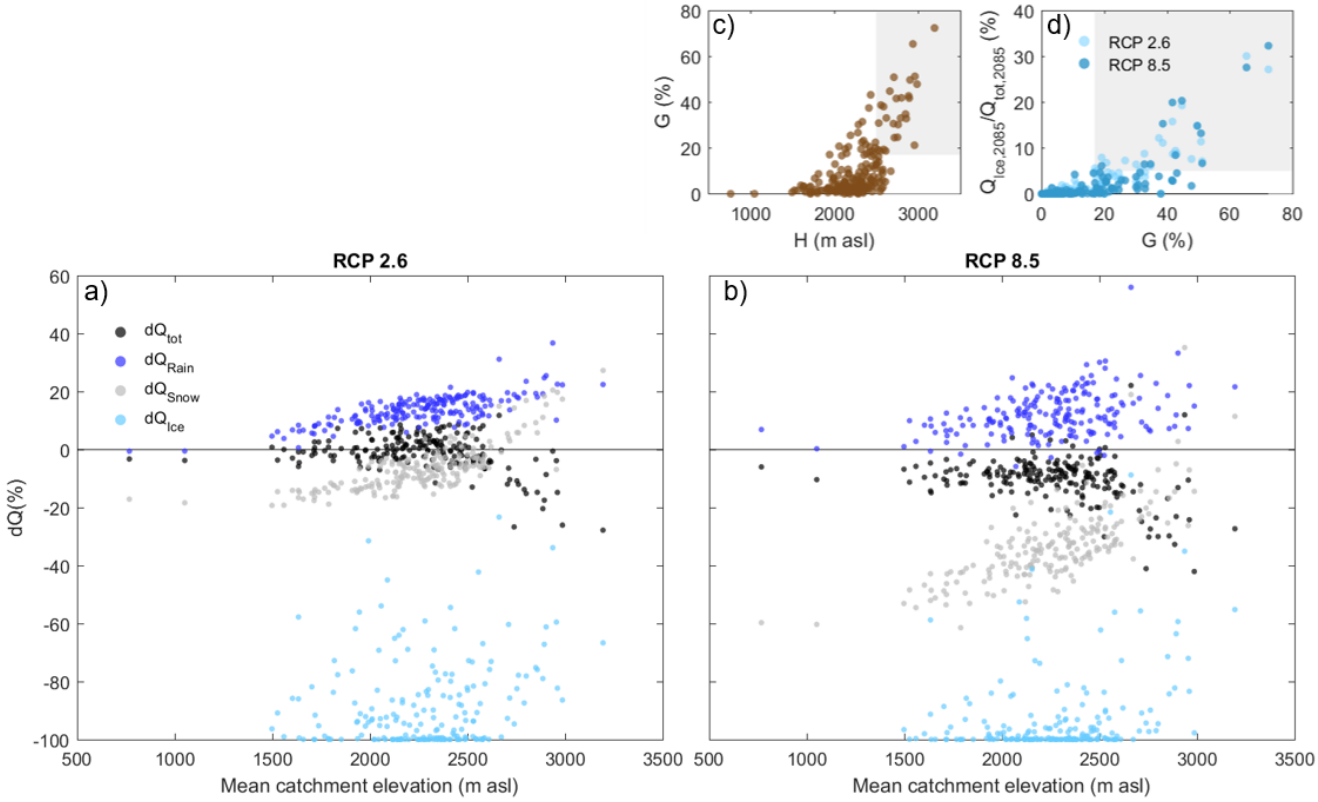

Figure 9: Mean changes in the annual total discharge (Q_{tot}) and in the annual contribution of rain (Q_{Rain}), snow (Q_{Snow}) and ice melt (Q_{Ice}) around 2085 compared to the mean catchment elevation for the emission scenarios RCP 2.6 (a) and RCP 8.5 (b). In (c), glacier coverage (G; situation in 1973) is plotted against mean catchment elevation (H) for all catchments and in (d), the percentage of the ice component in the total discharge at the end of the century ($Q_{Ice,\ 2085}/Q_{tot,\ 2085}$ x 100) is related to glacier coverage. The catchments with G>17% and H>2500 m asl, as well as $Q_{Ice,\ 2085}/Q_{tot,\ 2085}$ x 100>5% are highlighted with a grey background in (c) and (d), respectively.

Time series of annual discharge and discharge regime are presented in Figure 12 for Q_{tot}, Q_{Rain}, Q_{Snow} and Q_{Ice} and for three periods (reference period, around 2060, and around 2085) for four selected headwater catchments. In the most glacierized catchment at Gletsch (Rhone, Figure 12d), the annual contribution of ice melt might decrease from 26% of Q_{tot} in the reference period to 10% under RCP 2.6 and 4% under RCP 8.5 until the end of the century. Similar decreases can be observed for the catchments with medium glacier cover (Figures 12b-c). In the least glacierized catchment (Krummbach at Klusmatten, Figure 12a), the ice melt contribution to total discharge is already very small at the beginning of the simulation. In the four catchments, Q_{Snow} represents between 30 and 40% of total discharge in the reference period, the remaining amount of

snowmelt at the end of the century is highly variable between the catchments for RCP 8.5 with the least glacierized and lowest catchment (Figure 12a) experiencing the largest loss of Q_{Snow} with almost -20% units and the other catchments with Q_{Snow} losses between -9 and -5% units. As observed in Figures 10 and 11, Q_{Snow} changes are rather small under RCP 2.6 and even positive in Pontresina and Gletsch (Figure 12b and d).

The nivo-pluvial discharge regime at Klusmatten for the reference period might become mostly influenced by rain around 2085, and the loss in snowmelt will lead to smaller discharge peaks in spring (Figure 12a). In Pontresina and Kandersteg (Figure 12b-c), discharge regimes will experience a shift from a rather glacio-nival to a rather nivo-pluvial regime until the end of the century for RCP 8.5, and the discharge peak might decrease and occur earlier. At Gletsch (Figure 12d), the glacio-nival regime might remain until the end of the century, but losses in snow and glacier melt components may induce earlier and smaller discharge peaks.

In Table 3, the total annual contribution of Q_{Rain}, Q_{Snow} and Q_{Ice} to the total discharge was summed up for all headwater catchments of the Inn, Ticino, Rhone, and Rhine River basins for RCP 2.6 and RCP 8.5, the reference period and the end of the century (around 2085). Note that this only comprises the headwater catchments modelled in this study and is not representative of the actual total discharge of the given river basins. Most impacted is the Rhone River basin with up to -12.6% of Q_{tot} compared to the reference period under RCP 8.5. This can partly be explained by the large loss in glacier melt contribution with Q_{ice} contribution of 18.1% during the reference period and only 6.6% around 2085. The River basins Ticino, Inn and Rhine experience the largest changes in snowmelt contribution that will only be partly compensated by an increase in rain contribution on the annual scale. However, these changes in snowmelt and rain contribution have a large impact on the seasonality and might lead to a shift of the discharge peak (see Section 5.2). Only in Ticino and under scenario RCP 2.6 a positive impact on the total discharge is expected (+4.9% units), mainly due to an increase in the rain contribution and a smaller difference in the snowmelt contribution between the end of the century and the reference period compared to RCP 8.5.

Table 3: Total annual contribution of rain (Q_{Rain}), snow (Q_{Snow}) and ice melt (Q_{Ice}) as percentage of the total discharge Q_{tot} and as the sum for all headwater catchments of the Inn, Ticino, Rhone and Rhine River basins. Note that this only comprises the headwater catchments modelled in this study and is not representative of the actual total discharge of the river basins. The results are presented for the reference period and the 30-period centred at 2085 for RCP 2.5 and RCP 8.5. ΔQ_{tot} is the change in total discharge compared to the reference period.

		Q_{Rain} (%)		Q_{Snow} (%)		Q_{Ice} (%)		Q_{tot} (m^3/s)	ΔQ_{tot} (% unit)
		ref	2085	ref	2085	ref	2085	ref	2085
Inn	*RCP 2.6*	61.6	69.0	32.8	30.5	5.7	0.7	33.5	-1.4
	RCP 8.5	57.7	71.2	36.6	27.6	5.7	0.8	33.2	-9.5
Ticino	*RCP 2.6*	72.4	78.8	24.9	21.0	2.7	0.3	55.8	+4.9
	RCP 8.5	71.3	85.2	26.1	14.6	2.7	0.2	55.5	-6.9
Rhone	*RCP 2.6*	45.8	56.7	35.6	37.1	18.1	6.6	146.8	-5.3
	RCP 8.5	44.8	60.5	37.4	32.5	18.1	6.6	146.2	-12.6
Rhine	*RCP 2.6*	65.4	72.3	29.6	26.1	4.9	1.5	320.2	-1.8
	RCP 8.5	64.5	78.7	30.6	20.0	5.0	0.9	317.8	-7.6

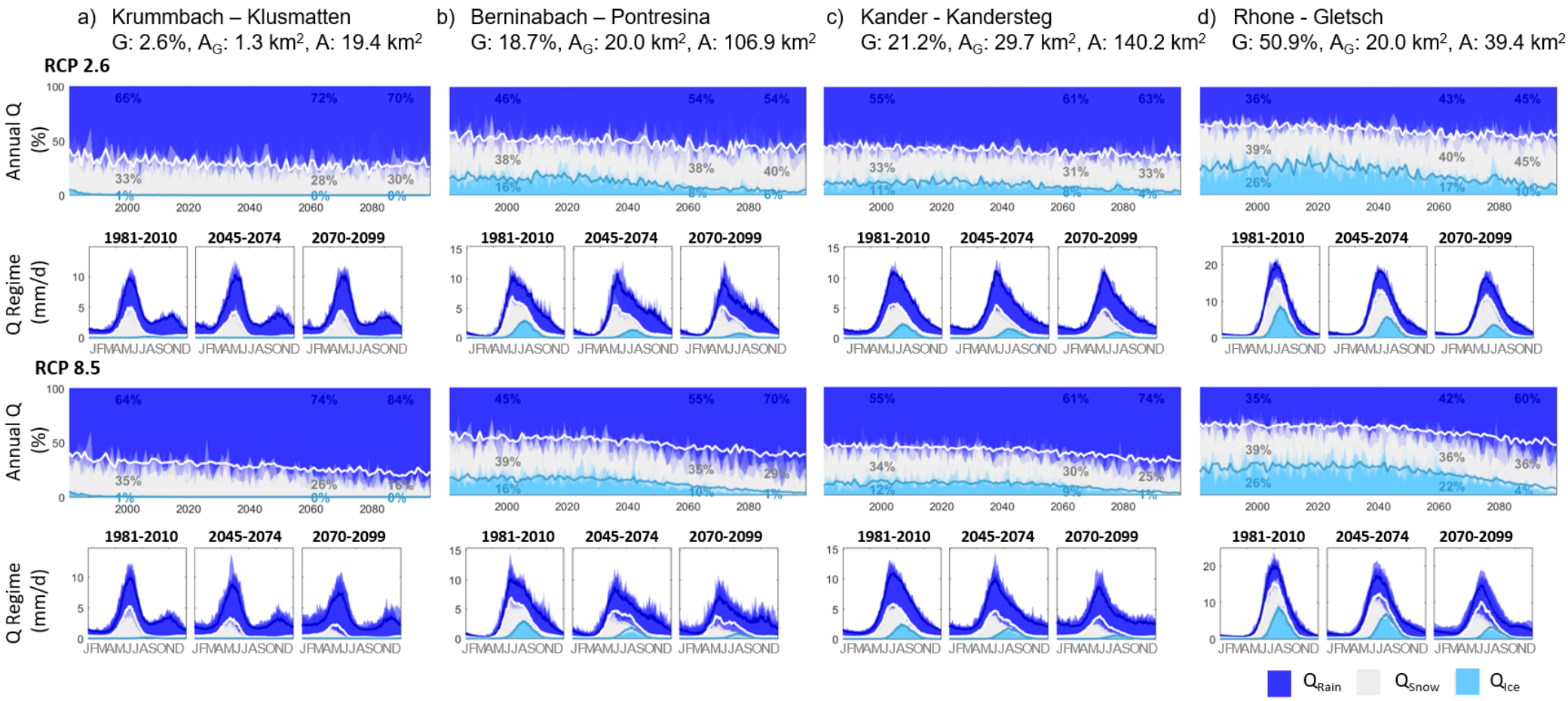

Figure 10: Time series of the annual contribution of rain (Q_{Rain}), snow (Q_{Snow}) and ice melt (Q_{Ice}) as percentage of Q_{tot} as well as the absolute discharge regime as a mean for three 30-yr periods for emission scenarios RCP 2.6 and RCP 8.5 as an example for four selected catchments with increasing glacier cover (from right to left) to show the different impacts of the discharge components depending on the catchment characteristics. The single climate model runs are shown in transparency in the background (9 for RCP 2.6 and 21 for RCP 8.5), the ensemble median is shown as a bold line.

Take home message from the changes in discharge components

- While annual total discharge might only marginally change under climate change conditions, the single discharge components might experience large changes until the end of the century that differ spatially.

- The glacier melt component will decrease on average by more than 90% units compared to the reference period at the end of the century, with only little differences between the emission scenarios as glaciers react with delay to climate change. The glacier melt component won't represent more than 2% on average of the total discharge for all headwater catchments around 2085.

  The rain component is expected to increase from ca. 60% of total discharge during the reference period to ca. 69% and ca. 74% under RCP 2.6 and RCP 8.5, respectively, until the end of the century on average for all catchments. For these changes large regional differences have to be considerred.
- The snowmelt component shows the largest difference between emission scenarios RCP 2.6 and RCP 8.5 and represents a significant part of the total discharge, especially at high altitudes. Snowmelt contribution to total discharge is expected to decrease from ca. 31% of total discharge during the reference period to ca. 29% and ca. 23% under RCP 2.6 and RCP 8.5, respectively, until the end of the century on average for all catchments. However large regional differences are expected. Limiting our impact on climate would allow to minimize losses in snowmelt contribution to discharge and minimize the expected changes in seasonality.

5.2 Changes in discharge seasonality

As already pointed out in Section 5.1, changes in seasonality of the discharge regimes are expected in nearly all catchments between the reference period and the end of the century, but the intensity of these changes varies depending on several factors, e.g. the original glacier cover and mean catchment elevation. In Figure 13, the changes in total discharge in 2085 compared to the reference period were assessed for the 195 headwater catchments for four seasons under RCP 2.6 and RCP 8.5 emission scenarios and compared to the mean catchment elevation. Strong positive elevation dependency can be observed in spring. This is due to snowmelt contribution shifted to earlier times and an increase of the liquid precipitation (see also Figure 14; CH2018, 2018). In the summer months, a decrease of total discharge can be observed for all catchments independently of the elevation, mainly due to a shift in snowmelt events, a loss of glacier melt, and less rainfall in the summer months (e.g. CH2018, 2018). Autumn shows overall a small decrease in total discharge but no trends related to elevation. The winter months show overall an increase in total discharge, due to earlier snowmelt and more frequent rainfall events in winter (e.g. CH2018, 2018). Overall, changes in the seasonality of Q_{tot} are stronger for RCP 8.5 than RCP 2.6.

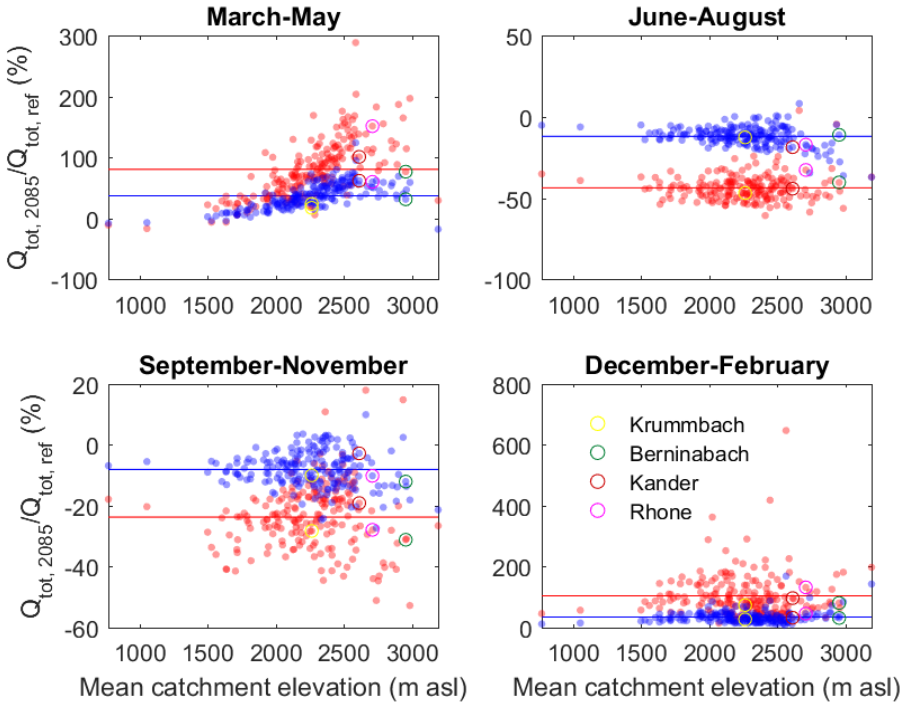

Figure 11: Percentual changes in monthly total discharge for four seasons for all 195 headwater catchments depending on elevation for emission scenarios RCP 2.6 (blue) and RCP 8.5 (red). The 30-yr period centred at 2085 is compared to the reference period. The horizontal line is the mean value for all catchments. The dots corresponding to the selected catchments from Figure 9 are highlighted with colour.

In Figure 14a-d, the mean discharge regime is compared for the reference period and around 2060 and 2085 under emission scenario RCP 8.5 for four selected catchments. For clarity reasons, only the median of all climate model runs is plotted as a 30-days moving average. The seasonal shifts in Q_{tot} observed in Figure 13 can be well observed in the four catchments. Such a shift of the maximum discharge from summer to spring was also found in other studies (e.g. Beniston, 2003; Farinotti *et al.*, 2012; Hanzer *et al.*, 2018). Smaller peaks in summer are due to a decrease of the glacier melt peaks and an earlier occurrence of the snowmelt peak. In summer, Q_{Rain} is expected to increase in the Krummbach catchment (Figure 14a) and to decrease or to stay equal in the other catchments (Figure 14b-c) that are located at higher elevations. Larger Q_{tot} in spring can be related to an earlier start of the snowmelt events and to an increase of the contribution of Q_{Rain}. In autumn, the decrease of Q_{tot} can be related to a shift of Q_{Snow} with snowmelt events ending earlier in the year as well as smaller peaks in the glacier melt contribution and a small shift of Q_{Ice} for the higher glacierized catchments. Q_{Rain} is expected to become more variable for all catchments.

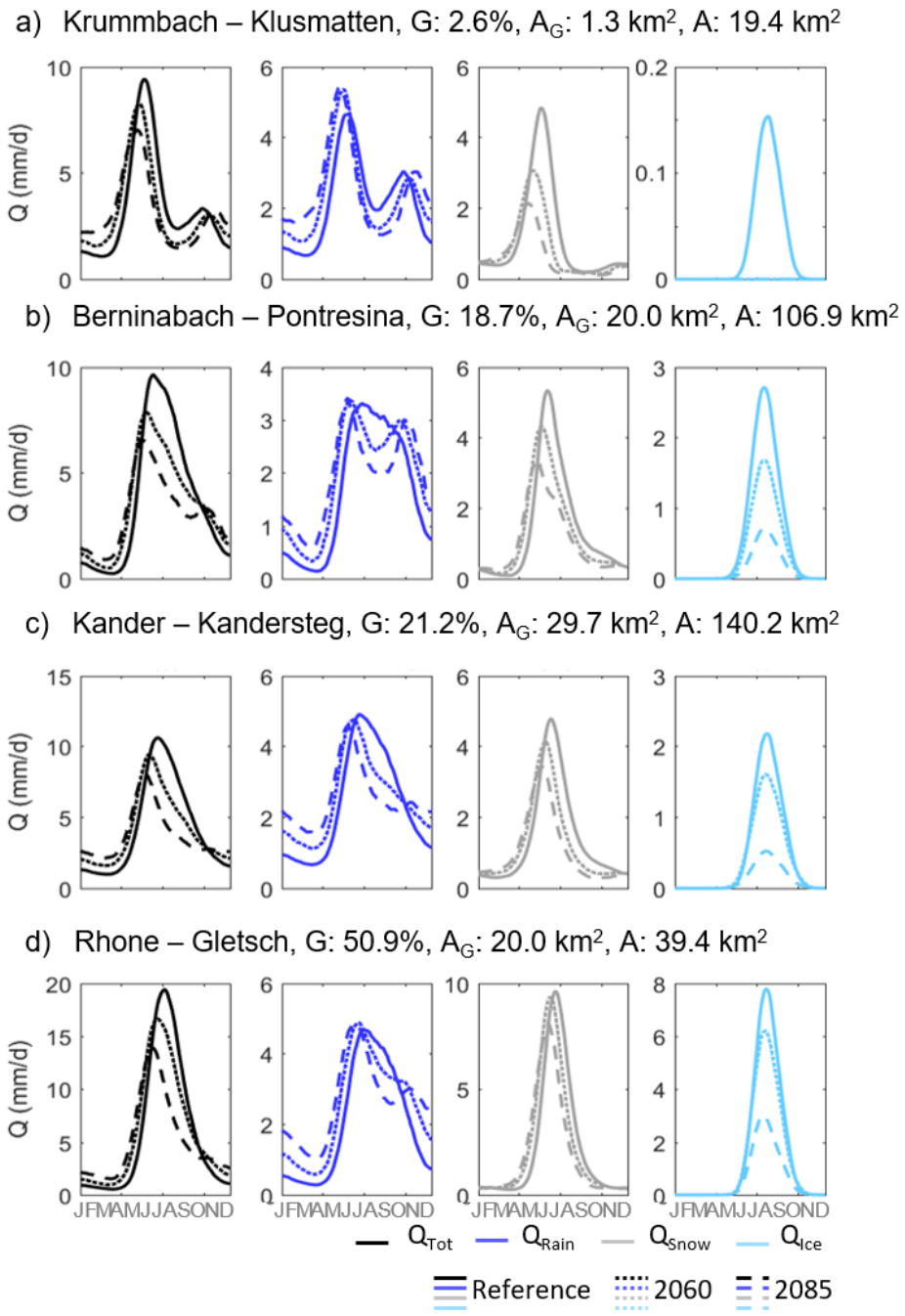

Figure 12: Comparison of the seasonality of the total discharge (Q_{tot}) and the contribution of rain (Q_{Rain}), snow (Q_{Snow}) and ice melt (Q_{Ice}) for three 30-yr periods of the emission scenario RCP 8.5. The ensemble median (21 climate models) of the 30-yr mean is presented as a 30-days moving average. Note that the scale of the y-axis differs between the graphs.

Under climate change, not only changes in discharge regime are expected but the inter-annual variability, meaning the year to year variability of the discharge, is also expected to change. To assess changes in inter-annual variability, we calculated the difference between the maximum and the minimum annual discharge over a moving 30-yr period for four seasons and for four chosen catchments. This difference is an indicator for the inter-annual variability over a given period, the larger the difference, the larger the inter-annual variability. Results show that the inter-annual variability becomes larger in the winter months for the four catchments (Figure 15a-d). This can be related to an increase in rainfall events in winter, due to the combined effect of increased winter precipitations and temperatures compared to the reference period (CH2018, 2018). The inter-annual variability in the summer months is expected to stay stable or slightly decrease, especially in highly glacierized catchments such as the Rhone at Gletsch (Figure 15d), due to the loss of glacier melt contribution as well as a reduction of precipitation in summer (CH2018, 2018). The inter-annual variability of spring and

autumn discharge is expected to stay rather stable or slightly increase for all catchments, but the highly glacierized catchment of the Rhone at Gletsch. The slightly increases might be explained by a combined effect of smaller snowmelt events and more extreme rainfall events (CH2018, 2018). The first small increase until 2030 and then reduction of the inter-annual variability in the Rhone catchment at Gletsch is due to the changes in seasonality and reduction of the snowmelt and glacier melt events. In the Rhone catchment, the variability of the spring and autumn discharge is expected to decrease slightly.

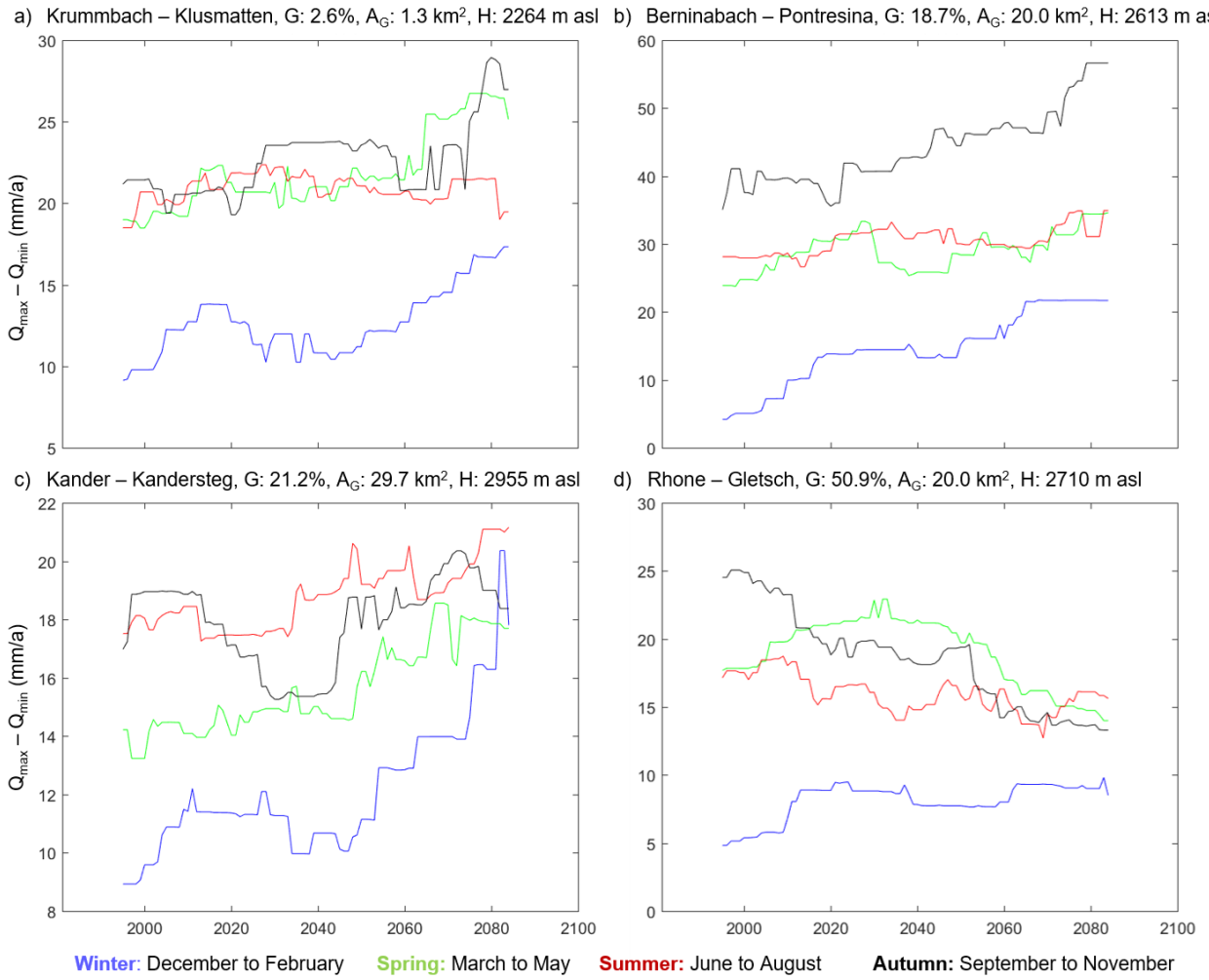

Figure 13: Inter-annual variability of the maximum of the total monthly discharge. The difference between the maximum (Qmax) and the minimum (Qmin) annual discharge over a moving 30-yr period was calculated for all climate models and for four seasons. The median of this difference is plotted here for the emission scenario RCP 8.5 and for four chosen catchments.

Take home message from the changes in seasonality

- The changes of discharge components will lead to a shift of the discharge seasonality with discharge peaks occurring earlier due to earlier snowmelt melt events.
- The discharge peaks are also expected to become smaller, due to negative changes in snowmelt and glacier melt contribution to discharge.
- These seasonal changes in discharge regime vary regionally depending on, e.g. the mean catchment elevation or the glacier cover at the beginning of the simulation.

5.3 Is peak water already reached in Switzerland?

Finding the timing of the peak water in glacierized catchments is a very actual topic and most studies found that in the European Alps, peak water was already reached or will be reached in the next decades (e.g. Farinotti *et al.*, 2012b; Beniston *et al.*, 2018; Huss and Hock, 2018). While most studies define peak water as the maximum of the glacier runoff, it is interesting to also analyse the maximum discharge for the different discharge components and for the total discharge, as even if the peak water is reached for the glacier runoff, the non-glacierized part of the catchment might play a significant role, and the glacier peak water might not be visible in the total discharge. In this study, we estimated the timing of the maximum of the discharge components rain, snow and ice melt as well as the total discharge for the median of all climate models for RCP 2.6 and RCP 8.5 (Figure 16a-d). One has to note that the ice melt component corresponds only to the runoff generated by melted ice and is not the glacier runoff (rain, snow and ice melt from the glacier area).

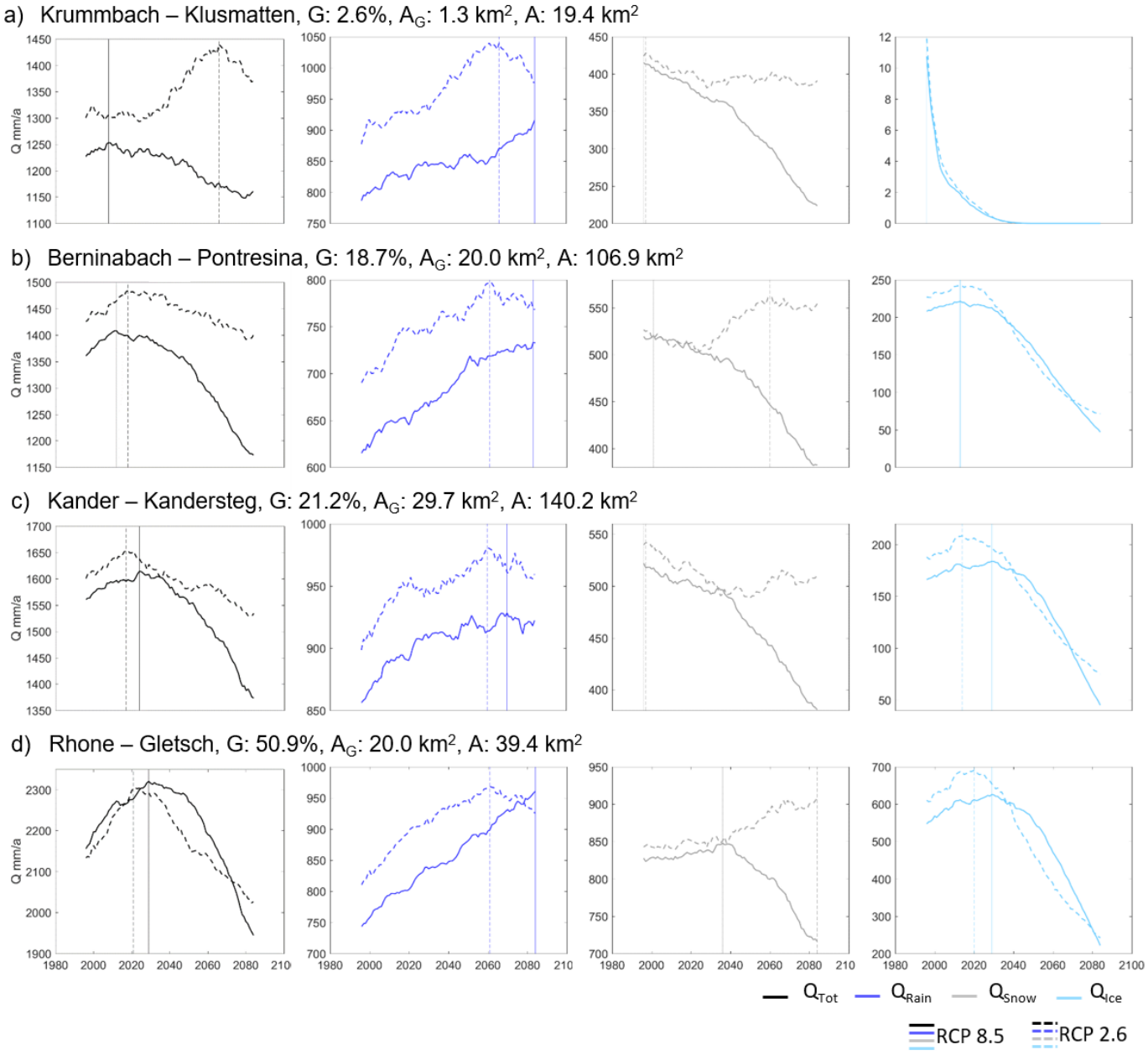

Figure 14: Comparison of the annual sum of the total discharge (Q_{tot}) and the contribution of rain (Q_{Rain}), snow (Q_{Snow}) and ice melt (Q_{Ice}) for two emission scenario RCP 2.6 and RCP 8.5. The ensemble median (9 and 21 climate models for RCP 2.6 and RCP 8.5 resp.) with a 30-yr moving average is shown in the figures. The vertical line indicates the occurrence of the maximum discharge for the given emission scenario. Note the different scales of the y-axis.

One challenge in finding the occurrence of the maximum discharge is that the time series need to be smoothed to minimize the impact of the year to year variability. However, the choice of the smoothing method has a large impact on the final results. In this study, we decided to smooth the time series with a 30-year moving average as we compare the contribution for 30-year periods. To test the impact of the choice of the moving average period on the estimation of the timing of the peak water, we also used a moving average of 10 years (not shown here). The comparison of the two smoothing methods showed a variation of +- 20 years between the estimated years of the peak water. This little experiment shows that the results of this analysis have to be interpreted carefully and are only an indication of a possible timescale for the occurrence of the maximum discharge. Furthermore, even with a smoothed time series, the discharge time series can be rather flat around the maximum, and the exact location of the maximum is difficult to define.

In Figure 16a-d, the ensemble median for the annual sum of Q_{tot}, Q_{Rain}, Q_{Snow}, and Q_{Ice} is presented for four selected catchments for RCP 2.6 and RCP 8.5 from 1981 to 2099. When identifiable, the maximum discharge is shown with a vertical line. For the catchments of the Berninabach, the Kander and the Rhone rivers (Figure 16b-d), maximum Q_{tot} is clearly identifiable and corresponds well to the maximum Q_{Ice}. It occurs for both emission scenarios before 2030. Maximum discharge in Q_{Ice} occurred at the Krummbach catchment before the start of the time series. The maximum discharge in Q_{tot} strongly varies between RCP 2.6 and RCP 8.5, which is due to the combined effect of increasing Q_{Rain} for both scenarios and slightly and largely decreasing Q_{Snow} for RCP 2.6 and RCP 8.5 until the end of the century. As already observed in Section 5.1 and Section 5.2, the largest differences between both emission scenarios are related to the snowmelt discharge component, which shows opposite trends for all catchments between RCP 2.6 and RCP 8.5 after 2040. This can be explained by the difference in temperature increase between both emission scenarios. Both scenarios show similar temperature increases until 2040, but until the end of the century, the temperature is expected to increase on average for Switzerland between +0.6 and +1.9°C under RCP 2.6 and between +3.3 and +5.4°C under RCP 8.5 (CH2018, 2018). Furthermore, winter precipitation is expected to increase under both scenarios (CH2018, 2018). Under RCP 2.6 and at high elevations, temperatures might be cold enough even at the end of the century for the winter precipitation to fall in the form of snow, leading to an increase in Q_{Snow} after 2040. In contrary, under RCP 8.5, most of the winter precipitation will fall in the form of rain, leading to a decrease in Q_{Snow}.

Take home message from the peak water

- Peak water is challenging to assess as its definition is unclear and it depends on the smoothing method used on the time series.
- Maximum glacier melt has already been reached by most of the catchments or will be reached within the next 20 years.
- The maximum in total discharge does not always coincide with the maximum in glacier melt and might be influenced by changes in snowmelt contribution and increases in rain contribution.

6. Conclusions

Using a broad range of observed data and a multi-criteria calibration method combined to a regionalization approach allowed us to successfully estimate the contribution of rain, snow and glacier melt to total discharge for 195 glacierized headwater catchments in the Swiss Alps for present and future climate under three emission scenarios (RCP 2.6, RCP 4.5 and RCP 8.5). We analyzed different aspects of the simulated hydrographs to understand the expected changes until the end of the century. While annual total discharge may only marginally change under climate change conditions, the single discharge components will experience large changes that differ spatially. The largest negative changes in total discharge are expected for catchment above 2500 m asl and with glacier cover larger than 17% at the start of the simulation, and can be related to the loss of glacier melt contribution.

The contribution of glacier melt will decrease on average for all catchments by more than 90% compared to the reference period until the end of the century, with only little differences between the emission scenarios as glaciers react with delay to climate and even the best-case scenario would not allow to slow down the glacier retreat significantly. On average for all glacierized catchments, glacier melt contribution won´t represent more than 2% of the total discharge around 2085. With ca. 18% Q_{Ice}, the Rhone River basin has the highest contribution of glacier melt during the reference period, but this contribution will decrease to less than 7% until the end of the century. This will largely influence the total discharge of the headwater catchments of the Rhone River basin, and Q_{tot} might experience a decrease of up to -13% until the end of the century and under RCP 8.5. Especially in the Rhine, Inn and Ticino River basins, the snowmelt contribution to discharge shows the largest differences between emission scenarios RCP 2.6 and RCP 8.5 and represents a significant part of the total discharge, in particular at high altitudes. These differences are due to the expected increase of winter precipitation in combination with the large differences in temperature increase under best-case and worst-case scenarios. Limiting the human impacts on the climate would allow to partly minimize losses in snowmelt contribution to discharge and, thus, minimize the expected changes in seasonality. In all river basins, the rainfall contribution to discharge is likely to increase on average for the entire year. However seasonal differences are expected with large increases in winter and decreases in summer.

Peak water is challenging to assess as its definition is unclear, and it depends on the smoothing method applied to the time series. Maximum glacier melt has already been reached by most of the catchments or will be reached before 2050. The maximum in total discharge does not always coincide with the maximum in glacier melt contribution and is largely influenced by changes in snowmelt contribution and increases in the rain component.

The changes in the contribution of rain, snow and glacier melt to total discharge will lead to a shift in the discharge seasonality, with annual maximum occurring earlier in the year, due to earlier snowmelt and glacier melt events. The discharge peaks are also expected to become smaller, due to negative changes in snowmelt and glacier melt contribution to discharge. However, these changes in discharge regime vary regionally depending on, e.g., the mean catchment elevation or the glacier cover at the beginning of the simulation. The discharge regime is expected to change from a rather glacio-nival to a rather nivo-pluvial regime for most of the highly glacierized catchments.

To conclude, future discharge is expected to slightly decrease, but, most importantly, the seasonal patterns will change, relying less on the well-predictable snowmelt and glacier melt contributions and more on the stochastic rain contribution. These seasonal changes will affect the water availability in Switzerland, especially during drought summers, when a reduction of the rain, snow and glacier melt contributions is expected. These changes need to be taken into account for the management of future water resources.

Acknowledgements

We thank K. Stahl, M. Weiler, I. Kohn, M. Van Tiel and B. Schaefli for their valuable help and advice during the project. We thank the FOEN, the Cantons Bern, Ticino, St. Gallen and Glarus, AlpiQ, OFIMA, H. Huwald, M. Huss, N. Griessinger, T. Jonas and S. Fugger for providing us with data for model calibration. The project is part of Hydro-CH2018 and was financed by FOEN.

References

Addor, N., Rössler, O., Köplin, N., Huss, M., Weingartner, R., and Seibert, J. (2014) 'Robust changes and sources of uncertainty in the projected hydrological regimes of Swiss catchments', *Water Resources Research*, pp. 1–22. doi: 10.1002/2014WR015549.

Allen, R. G., Pereira, L.S., Raes, D., and Smith, M. (1998) '*Crop evapotranspiration – Guidelines for computing crop water requirements', FAO Irrigation and drainage paper 56,* Food and Agriculture Organization, Rome.

BAFU (2021) '*Auswirkungen des Klimawandels auf die Schweizer Gewässer*'. *Hydrologie, Gewässerökologie und Wasserwirtschaft. Bundesamt für Umwelt BAFU, Bern. Umwelt-Wissen Nr. 2016: XXpp*.

Bard, A., Renard, B., Lang, M., Giuntoli, I., Korck, J., Koboltschnig, G., Janža, M., Amico, M., and Volken, D. (2015) 'Trends in the hydrologic regime of Alpine rivers', *Journal of Hydrology*, 529, pp. 1823–1837. doi: 10.1016/j.jhydrol.2015.07.052.

Belz, J. U., Brahmer, G., Buiteveld, H., Engel, H., Grabher, R., Hodel, H., Krahe, P., Lammersen, R., Larina, M., Mendel, H.-G, Meuser, A., Müller, G., Plonka, B., Pfister, L., and van Vuuren, W. (2007) '*Das Abflussregime des Rheins und seiner Nebenflüsse im 20. Jahrhundert*'. Report Nr. I-22, International Commission for the Hydrology of the Rhine Basin, ISBN 978-90-70980-33-7, 377pp.

Beniston, M. (2003) *'Climatic Change in Mountain Regions: A Review of Possible Impacts, in: Climate Variability and Change in High Elevation Regions: Past, Present & Future'*, edited by Diaz, H., vol. 15 of Advances in Global Change Research, pp. 5–31, Springer Netherlands, doi:10.1007/978-94-015-1252-7 2.

Beniston, M., Farinotti, D., Stoffel, M., Andreassen, L. M., Coppola, E., Eckert, N., Fantini, A., Giacona, F., Hauck, C., Huss, M., Huwald, H., Lehning, M., López-Moreno, J. I., Magnusson, J., Marty, C., Morán-Tejéda, E., Morin, S., Naaim, M., Provenzale, A., Rabatel, A., Six, D., Stötter, J., Strasser, U., Terzago, S., and Vincent, C. (2018) 'The European mountain cryosphere: A review of its current state, trends, and future challenges', *Cryosphere*, 12(2), pp. 759–794. doi: 10.5194/tc-12-759-2018.

Bergström, S. (1976) '*Development and application of a conceptual runoff model for Scandinavian catchments'*. Hydrology repoort RHO 7, Swedisch Meteorological and Hydrological Institute Narrkoping, Sweden, 134pp.

Bittner, S. (2019) *Parametrisierung eines konzeptionnellen Schneeumverteilungsansatzes bei der Modellierung alpiner Einzugsgebiete,* Master Thesis, University of Freiburg, Germany, 151pp.

Brunner, M. I., Farinotti, D., Zekollari, H., Huss, M., and Zappa, M. (2019) 'Future shifts in extreme flow regimes in Alpine regions', *Hydrology and Earth System Sciences, 23, 4471-4489*, doi: 10.5194/hess-2019-144.

Carrivick, J. L. and Brewer, T. R. (2004) 'Improving local estimations and regional trends of glacier equilibrium line altitudes', *Geografiska Annaler, Series A: Physical Geography*. Blackwell Publishing Ltd, 86(1), pp. 67–79. doi: 10.1111/j.0435-3676.2004.00214.x.

CH2018 (2018) *Climate Scenarios for Switzerland, Technical Report, National Centre for Climate Services, Zurich, 271 pp. ISBN: 978-3-9525031-4-0*.

CH2018 project Team (2018) 'CH2018 - Climate Scenarios for Switzerland. National Centre for Climate Services. doi: 10.18751/Climate/Scenarios/CH2018/1.0'.

Duethmann, D. and Blöschl, G. (2018) 'Why has catchment evaporation increased in the past 40 years ? A data-based study in Austria', *Hydrology and Earth System Sciences*, 22, pp. 5143–5158. doi: 10.5194/hess-22-5143-2018.

Etter, S., Addor, N., Huss, M., and Finger, D. (2017) 'Climate change impacts on future snow, ice and rain runoff in a Swiss mountain catchment using multi-dataset calibration', *Journal of Hydrology: Regional Studies*. Elsevier, 13(September), pp. 222–239. doi: 10.1016/j.ejrh.2017.08.005.

Farinotti, D., Usselmann, S., Huss, M., Bauder, A., and Funk, M. (2012) 'Runoff evolution in the Swiss Alps: projections for selected high-alpine catchments based on ENSEMBLES scenarios', *Hydrological Processes*, 26(13), pp. 1909–1924. doi: 10.1002/hyp.8276.

Finger, D., Vis, M., Huss, M., and Seibert, J. (2015) 'The value of multiple data set calibration versus model complexity for improving the performance of hydrological models in mountain catchments', *Water Resources Research*, 51. doi: 10.1002/2014WR015712.

Fischer, M.,Huss, M., Barboux, C., Hoelzle, M. (2014) 'The new Swiss Glacier Inventory SGI2010: Relevance of using high-resolution source data in areas dominated by very small glaciers', *Arctic, Antarctic, and Alpine Research*, 46(4), pp. 933–945.

Frei, C. (2014) 'Interpolation of temperature in a mountainous region using nonlinear profiles and non-Euclidean distances', *International Journal of Climatology*, 34(5), pp. 1585–1605. doi: 10.1002/joc.3786.
Frei, C. and Schär, C. (1998) 'A precipitation climatology of the Alps from high-resolution rain-gauge observations', *International Journal of Climatology*, 18, pp. 873–900.
Frei, P., Kotlarski, S., Liniger, M. A., and Schär, C. (2018) 'Future snowfall in the Alps : projections based on the EURO-CORDEX regional climate models', Cryosphere, Vol. 12, pp. 1–24. DOI: 10.5194/tc-12-1-2018
Freudiger, D., Frielingsdorf, B., Stahl, K., Steinbrich, A., Weiler, M., Griessinger, N., and Seibert, J. (2016) 'Das Potential meteorologischer Rasterdatensätze für die Modellierung der Schneedecke alpiner Einzugsgebiete', *Hydrologie und Wasserbewirtschaftung*, 60(6), pp. 353–367. doi: 10.5675/HyWa.
Freudiger, D., Kohn, I., Seibert, J., Stahl, K., and Weiler, M. (2017) 'Snow redistribution for the hydrological modeling of alpine catchments', *Wires Water*, pp. 1–16. doi: 10.1002/wat2.1232.
Hall, D. and Riggs, G. (2016) 'MODIS/Terra Snow Cover Daily L3 Global 0.05 Deg CMG, Version 6, Boulder USA, NASA National Snow and Ice Data Center Distributed Active Archive Center'.
Hamon, W. R. (1963) 'Computation of direct runoff amounts from storm rainfall', *Int. Assoc. Sci. Hydrol. Publ.*, (63), pp. 52–62.
Hanzer, F., Förster, K., Nemec, J., and Strasser, U. (2018): '*Projected cryospheric and hydrological impacts of 21st century climate change in the Ötztal Alps (Austria) simulated using a physi- cally based approach'*, Hydrol. Earth Syst. Sci., 22, 1593–1614, https://doi.org/10.5194/hess-22-1593-2018.
Hrachowitz, M., Fugger, S. and Schulz, K. (2020) 'Regional pattern of annual snow cover duration in the Greater Alpine Region (2000 - 2018)', in *22nd EGU General Assembly, held online 4-8 May, 2020, id.4863*.
Huss, M., Jouvet, G., Farinotti, D., and Bauder, A. (2010) 'Future high-mountain hydrology: a new parameterization of glacier retreat', *Hydrology and Earth System Sciences*, 14(5), pp. 815–829. doi: 10.5194/hess-14-815-2010.
Huss, M. (2011) 'Present and future contribution of glacier storage change to runoff from macroscale drainage basins in Europe', *Water Resources Research*, 47(7), pp. 1–14. doi: 10.1029/2010WR010299.
Huss, M., Bookhagen, B., Huggel, C., Jacobsen, D., Bradley, R., Clague, J., Vuille, M., Buytaert, W., Cayan, D., Greenwood, G., Mark, B., Milner, A., Weingartner, R., and Winder, M. (2017) 'Towards mountains without permanent snow and ice', Earth 's Future, 5, pp. 418–435. doi: 10.1002/eft2.207.
Huss, M. and Fischer, M. (2016) 'Sensitivity of Very Small Glaciers in the Swiss Alps to Future Climate Change', *Frontiers in Earth Science*, 4, pp. 1–17. doi: 10.3389/feart.2016.00034.
Huss, M. and Hock, R. (2018) 'Global-scale hydrological response to future glacier mass loss', *Nature Climate Change*, 8, doi: 10.1038/s41558-017-0049-x.
Isotta, F. A., Frei, C., Weilguni, V., Perčec Tadić, M., Lassègues, P., Rudolf, B., Pavan, V., Cacciamani, C., Antolini, G., Ratto, S. M., Munari, M., Micheletti, S., Bonati, V., Lussana, C., Ronchi, C., Panettieri, E., Marigo, G., and Vertačnik, G. (2014) 'The climate of daily precipitation in the Alps: development and analysis of a high-resolution grid dataset from pan-Alpine rain-gauge data', *International Journal of Climatology*, 34(5), pp. 1657–1675. doi: 10.1002/joc.3794.
Jonas, T., Marty, C. and Magnusson, J. (2009) 'Estimating the snow water equivalent from snow depth measurements in the Swiss Alps', *Journal of Hydrology*. Elsevier B.V., 378(1–2), pp. 161–167. doi: 10.1016/j.jhydrol.2009.09.021.
Koboltschnig, G. R., Schöner, W., Zappa, M., and Holzmann, H. (2007) 'Contribution of glacier melt to stream runoff: If the climatically extreme summer of 2003 had happened in 1979...', *Annals of Glaciology*, 46, pp. 303–308. doi: 10.3189/172756407782871260.
Konz, M. and Seibert, J. (2010) 'On the value of glacier mass balances for hydrological model calibration', *Journal of Hydrology*, 385(1–4), pp. 238–246. doi: 10.1016/j.jhydrol.2010.02.025.
Krajčí, P., Holko, L., Perdigão, R. A.P., and Parajka, J. (2014) 'Estimation of regional snowline elevation (RSLE) from MODIS images for seasonally snow covered mountain basins', *Journal of Hydrology*, 519, pp. 1769–1778. doi: 10.1016/j.jhydrol.2014.08.064.
Maisch, M., Wipf, A., Denneler, B., Battaglia, J., and Benz, C. (2000) 'Die Gletscher der Schweizer Alpen: Gletscherstand 1850. Aktuelle Vergletscherung, Gletscherschwundszenarien. End report NFP 31, Second Edition, Zurich, vdf Hochschulverlag, ETH Zurich, 373 p.'
'Model Description - WaSiM (Water balance Simulation Model)' (2015) *Technical Report, Hydrology Software Consulting J Schulla, Regensdorfstrasse 162, CH-8049 Zurich, Switzerland.*, last exten, p. 318.
Müller, F., Caflish, T. and Müller, G. (1976) 'Firn und Eis der Schweizer Alpen, Gletscherinventar. Zurich vdf Hochschulverlag ETH Zurich, 373p.'
Mutzner, R., Weijs, S. V. , Tarolli, P., Calaf, M., Oldroyd, H. J. and Parlange, M. B. (2015) 'Controls on the diurnal streamflow cycles in two subbasins of an alpine headwater catchment', Water Resources Research, 51, 3403–3418, doi:10.1002/2014WR016581.
Oudin, L., Hervieu, F., Michel, C., Perrin, C., Andreassian, V., Anctil, F., and Loumagne, C. (2005) 'Which potential evapotranspiration input for a lumped rainfall–runoff model? Part 2—Towards a simple and efficient potential evapotranspiration model for rainfall–runoff modelling', *Journal of Hydrology*, 303(1–4), pp. 290–306. doi: 10.1016/j.jhydrol.2004.08.026.

Rauthe, M., Steiner, H., Riediger, U., Mazurkiewicz, A., and Gratzki, A. (2013) 'A Central European precipitation climatology – Part I: Generation and validation of a high-resolution gridded daily data set (HYRAS)', *Meteorologische Zeitschrift*, 22(3), pp. 235–256. doi: 10.1127/0941-2948/2013/0436.
Salzmann, N., MacHguth, H. and Linsbauer, A. (2012) 'The Swiss Alpine glaciers' response to the global "2°C air temperature target"', *Environmental Research Letters*, 7(4). doi: 10.1088/1748-9326/7/4/044001.
Schädler, B. and Weingartner, R. (2002) 'Ein detaillierter hydrologischer Blick auf die Wasserressourcen der Schweiz - Niederschlagskartierung im Gebirge als Herausforderung', *Wasser Energie Luft, CH 5401 Baden*, 94(7/8), pp. 189–197.
Schwarb, M. (2000) *The Alpine Precipitation Climate: Evaluation of a high-resolution analysis scheme using comprehensive rain-gauge data*. ETH, Zurich.
Seibert, J. (2000) 'Multi-criteria calibration of a conceptual runoff model using a genetic algorithm', *Hydrology and Earth System Sciences*, 4(2), pp. 215–224. doi: 10.5194/hess-4-215-2000.
Seibert, J., Vis, M. J. P., Kohn, I., Weiler, M., and Stahl, K. (2017) 'Technical Note: Representing glacier dynamics in a semi-distributed hydrological model', *Hydrology and Earth System Sciences Discussions*, 3, pp. 1–20. doi: 10.5194/hess-2017-158.
Seibert, J. and Vis, M. J. P. (2012) 'Teaching hydrological modeling with a user-friendly catchment-runoff-model software package', *Hydrology and Earth System Sciences*, 16(9), pp. 3315–3325. doi: 10.5194/hess-16-3315-2012.
Serquet, G., Marty, C., Dulex, J. P., and Rebetez, M. (2011) 'Seasonal trends and temperature dependence of the snowfall/precipitation- day ratio in Switzerland', *Geophysical Research Letters*, 38(7), pp. 14–18. doi: 10.1029/2011GL046976.
Simoni, S., Padoan, S., Nadeau, D., Diebold, M., Porporato, A., Barrenetxea, G., Ingelrest, F., Vetterli, M., and Parlange, M. (2011) 'Hydrologic response of an alpine watershed: Application of a meteorological wireless sensor network to understand streamflow generation', *Water Resourources Research*, 47, W10524, doi:10.1029/2011WR010730
Stahl, K., Moore, R. D., Shea, J. M., Hutchinson, D., and Cannon, a. J. (2008) 'Coupled modelling of glacier and streamflow response to future climate scenarios', *Water Resources Research*, 44(2), doi: 10.1029/2007WR005956.
Stahl, K., Weiler, M., Kohn, I., Freudiger, D., Seibert, J., Vis, M., and Gerlinger, K. (2016) *The snow and glacier melt components of streamflow of the river Rhine and its tributaries considering the influence of climate change - Synthesis report*. Lelystad, The Netherlands. Available at: www.chr-khr.org/en/publications.
Stahl, K., Weiler, M., Freudiger, D., Kohn, I., Seibert, J., Vis, M., Gerlinger, K., and Böhm, M. (2017) *The snow and glacier melt components of streamflow of the river Rhine and its tributaries considering the influence of climate change. Final report to the International Commission for the Hydrology of the Rhine (CHR)*. Available at: www.chr-khr.org/en/publications.
Van Tiel, M., Stahl, K., Freudiger, D., and Seibert, J. (2020) 'Glacio-hydrological model calibtration and evaluation', *Wires Water (accepted)*. doi: 10.1002/wat2.1483.
Viviroli, D., Archer, D. R., Buytaert, W., Fowler, H. J., Greenwood, G. B., Hamlet, a. F., Huang, Y., Koboltschnig, G., Litaor, M. I., López-Moreno, J. I., Lorentz, S., Schädler, B., Schreier, H., Schwaiger, K., Vuille, M., and Woods, R. (2011) 'Climate change and mountain water resources: overview and recommendations for research, management and policy', *Hydrology and Earth System Sciences*, 15(2), pp. 471–504. doi: 10.5194/hess-15-471-2011.
De Vries, H., Lenderink, G. and Van Meijgaard, E. (2014) 'Future snowfall in western and central Europe projected with a high-resolution regional climate model ensemble', *Geophysical Research Letters*, 41(12), pp. 4294–4299. doi: 10.1002/2014GL059724.
Weijs, S. V., Mutzner, R. and Parlange, M. B. (2013) 'Could electrical conductivity replace water level in rating curves for alpine streams?', Water Resources Research, 49, 343–351, doi:10.1029/2012WR012181.
Weiler, M., Seibert, J. and Stahl, K. (2018) 'Magic components—why quantifying rain, snowmelt, and icemelt in river discharge is not easy', *Hydrological Processes*, 32(1), pp. 160–166. doi: 10.1002/hyp.11361.
Zekollari, H., Huss, M. and Farinotti, D. (2019) 'Modelling the future evolution of glaciers in the European Alps under the EURO-CORDEX RCM ensemble', *Cryosphere*, 13(4), pp. 1125–1146. doi: 10.5194/tc-13-1125-2019.
Zekollari, H., Huss, M. and Farinotti, D. (2020) 'On the Imbalance and Response Time of Glaciers in the European Alps', *Geophysical Research Letters*, 47(2), pp. 1–9. doi: 10.1029/2019GL085578.

APPENDIX A: Metadata of the 38 undisturbed gauged catchments

Table A 1: List of 38 undisturbed gauged catchments and their characteristics.

ID	Basin	Area	Elevation			Aspect	Climatic data			Glacier					Gauging Station					Comments	Source
			mean	min	max	catch. mean	mean Prec. sum	mean Temp.	Prec. corr. factor	Area (1973)	Cover (1973)	Cover (2003)	Cover (2010)	Mean aspect		Start of obs.	End of obs.	Nr. of years	Elev.		
		km²	m asl	m asl	m asl	-	mm/yr	°C	-	km²	%	%	%	-					m asl		
1002	Inn	26,9	2363	1508	3160	N	1186	-0,9	1,26	0,5	2,0	0,0	0,0	N	Ova da Cluozza - Zernez	1970	2017	48	1509		BAFU 2319
1004	Inn	106,9	2613	1804	4025	N	1489	-2,0	1,22	20,0	18,7	16,0	14,3	N	Berninabach (Ova da Bernina) - Pontresina	1970	2017	48	1804	Little influenced	BAFU 2262
1005	Inn	128,5	2187	1235	3021	N	1187	0,4	1,39	0,0	0,0	0,0	0,0		Rom - Muestair	1994	2017	24	1236	non-glacierized	BAFU 2617
1006	Inn	73,4	2546	1724	3260	NW	1226	-1,9	1,16	0,8	1,0	0,1	0,1	N	Chamuerabach (Ova Chamuera) - La Punt-Chamues	1970	2017	48	1720		BAFU 2263
2001	Ticino	36,6	2248	1458	3133	W	2182	-0,3	1,37	1,0	2,6	0,8	0,8	N	Bleniotal - Luzziona	1970	2017	48	1590	Water balance between lake area and water level.	TI-Privat
2004	Ticino	14,1	2287	1865	3022	S	1460	0,1	1,00	0,0	0,0	0,0	0,0		Poschiavino - La Roesa	1970	2017	48	1860	Non-glacierized	BAFU 2366
2005	Ticino	120,5	1926	747	3180	E	2003	2,2	1,17	0,7	0,6	0,3	0,2	SE	Calancasca - Buseno	1970	2017	46	746	Little influenced	BAFU 2474
2009	Ticino	33,7	2120	1460	2891	SE	2148	1,9	1,11	0,0	0,0	0,0	0,0	NE	Maggiatal - Sambuco	1970	2017	48	1461	Water balance between lake area and water level.	TI-Privat
2010	Ticino	19,4	2264	1794	3207	E	1843	1,3	1,25	0,5	2,6	0,4	0,4	N	Krummbach - Klusmatten	1970	2017	46	1795	Missing data: 1993-1995	BAFU 2244
3001	Rhone	38,4	2380	1385	3177	W	2076	-0,7	1,00	5,0	13,0	5,4	4,0	NW	Goneri - Oberwald	1990	2017	28	1385		BAFU 2607
3002	Rhone	39,4	2710	1758	3620	SW	2192	-2,4	1,09	20,0	50,9	44,4	41,7	S	Rhone (Rotten) - Gletsch	1970	2017	48	1761	Water power from 2017	BAFU 2268
3003	Rhone	77,4	2621	1517	3893	S	2202	-2,0	1,22	25,6	33,1	28,7	24,7	S	Lonza - Blatten	1970	2017	48	1520		BAFU 2269
3004	Rhone	195,5	2937	1448	4190	SE	2343	-3,0	1,00	127,8	65,4	60,8	56,5	SE	Massa - Blatten bei Naters	1970	2017	48	1446		BAFU 2161
3005	Rhone	18,9	2565	1800	3243	SE	2006	-0,2	1,00	1,9	10,0	6,8	5,7	E	Liene - Tseuzier, Lourantse	1970	1991	22	1795	22% missing data	BAFU 341
3006	Rhone	20,4	2412	1775	3193	N	1651	-0,8	1,00	0,7	3,5	0,8	0,6	NE	Val Ferret	2009	2013	4	1777	Only summer	H-Huwald
3008	Rhone	80,5	3194	1936	4629	NW	1592	-5,7	1,00	58,2	72,3	70,4	63,3	NW	Gorner glacier	1971	2017	47	2006		Alpiq
3009	Rhone	43,2	2986	1618	4177	NW	1545	-4,4	1,18	20,7	47,8	41,9	39,8	NW	Findel glacier	1981	2017	37	2480	Q measured below glacier and scaled to catch. area	Alpiq

ID	Basin	Area	Elevation			Aspect	Climatic data			Glacier					Gauging Station					Comments	Source
			mean	min	max	catch. mean	mean Prec. sum	mean Temp.	Prec. corr. factor	Area (1973)	Cover (1973)	Cover (2003)	Cover (2010)	Mean aspect		Start of obs.	End of obs.	Nr. of years	Elev.		
		km²	m asl	m asl	m asl	-	mm/yr	°C	-	km²	%	%	%	-					m asl		
4003	Rhine	179,9	2058	648	4085	N	1964	0,8	1,08	37,3	20,7	19,1	16,6	N	Schwarze Luetschine - Guendlischwand	1992	1999	8	653	incl: 4004	BE-A010
4004	Rhine	97,2	2413	959	4085	W	2180	-1,5	1,07	36,4	37,4	35,3	30,5	N	Schwarze Luetschine - Grindelwald	2016	2017	2	981		BE-A112
4005	Rhine	140,2	2955	1050	3695	N	1892	-0,3	1,17	29,7	21,2	19,2	17,7	N	Kander - Kandersteg	2007	2017	12	1168	incl: 4006, 4134	BE-A096
4006	Rhine	43,6	2556	1415	3695	W	1797	-1,8	1,05	16,9	38,7	35,3	32,7	W	Kander - Gasterntal, Staldi	1970	1983	14	1478		BAFU 2234
4007	Rhine	1701,6	768	358	2500	N	1457	7,7	1,04	0,0	0,0	0,0	0,0		Thur - Andelfingen	1970	2017	48	356	Non-glacierized	BAFU 2044
4009	Rhine	478,3	1051	436	2334	N	1622	6,5	1,00	0,0	0,0	0,0	0,0		Kleine Emme - Emmen	1970	2017	48	430	Non-glacierized	BAFU 2634
4010	Rhine	343,7	1634	774	3243	NW	1617	3,8	1,00	11,5	3,4	2,6	2,4	N	Simme - Oberwil	1970	2017	48	777	incl: 4019, 4116	BAFU 2151
4011	Rhine	218,3	1946	578	4085	N	1929	1,5	1,10	37,3	17,1	15,8	13,7	N	Lütschine - Gsteig (without Weisse Lütschine)	1970	2017	48	585	inflow: 4020, incl: 4003	BAFU 2109 - BAFU 2200
4012	Rhine	131,9	1853	815	3144	S	1914	2,1	1,12	2,1	1,6	0,7	0,6	N	Sernf Matt	2014	2017	5	817	incl: 4126, 4117	GL-26110599
4013	Rhine	107,9	1719	488	3291	SW	2223	2,6	1,23	3,5	3,2	1,8	1,5	N	Schächen - Bürglen, Galgenwäldli (Hauptstation)	1985	2017	33	490	Little influenced; incl: 4122, 4118	BAFU 2491
4015	Rhine	228,0	1603	442	3221	NW	2110	3,2	1,17	8,4	3,7	2,8	2,5	NW	Engelberger Aa - Buochs, Flugplatz	1970	2017	48	443	Little influenced	BAFU 2481
4016	Rhine	21,8	2447	1489	3159	SW	1599	-0,7	1,03	1,3	6,0	3,2	1,7	N	Somvixer Rhein - Somvix, Encardens	1970	2017	48	1490		BAFU 2430
4017	Rhine	20,7	2194	1021	3192	NE	2045	0,9	1,25	5,3	25,5	22,1	19,6	NE	Alpbach - Erstfeld, Bodenberg	1970	2017	48	1022		BAFU 2299
4018	Rhine	43,9	1812	772	2940	NE	2577	2,8	1,45	3,8	8,7	7,0	6,7	N	Grosstalbach - Isenthal	1970	2017	48	767		BAFU 2276
4019	Rhine	34,7	2335	1095	3243	NW	1867	-0,9	1,00	10,9	31,4	25,2	22,6	NW	Simme - Oberried/Lenk	1970	2017	48	1096		BAFU 2219
4020	Rhine	164,9	2149	649	4145	N	1876	0,5	1,00	29,1	17,6	16,0	13,1	N	Weisse Luetschine - Zweiluetschinen	1970	2017	48	650		BAFU 2200
4030	Rhine	12,7	2440	1246	3420	SE	1947	0,5	1,00	2,1	16,5	11,4	10,7	SE	Ferrerabach - Trun	1970	1990	21	1220		BAFU 2323
4032	Rhine	53,9	2357	1586	3396	NE	2185	-0,2	1,28	9,1	17,0	8,7	7,1	N	Hinterrhein - Hinterrhein	1970	2012	43	1584	station 2224 downstream	BAFU 2224 & BAFU 933
4033	Rhine	103,5	2339	1321	3295	W	2156	-0,2	1,60	8,0	7,7	4,7	4,3	NW	Landquart - Klosters	1970	2005	36	1317		BAFU 2413
4036	Rhine	42,9	2371	1680	3139	NW	1401	-0,5	1,41	1,0	2,4	1,0	0,7	NW	Dischmabach - Davos, Kriegsmatte	1970	2017	48	1668		BAFU 2327
4037	Rhine	30,3	1716	938	3026	E	1566	4,0	1,17	0,0	0,0	0,0	0,0	E	Görbsbach, Pfaeffers, Vaettis, Winkel	1986	2017	32	942	Non-glacierized	SG-3701

APPENDIX B: Comparison of calculation methods for potential evapotranspiration

We compared five different methods to calculate potential evapotranspiration (PET): the reference Penman-Monteith equation (standard method as given by FAO, Allen *et al.*, 1998), Hargreaves (Allen *et al.*, 1998), Hamon (Hamon, 1963), Hamon as implemented in WaSIM (Model Description - WaSiM, 2015), and Oudin (Oudin *et al.*, 2005). All equations are listed in Table B1. To calculate PET, we used meteorological data from 13 high elevated weather stations located close to our headwater catchments. The stations were chosen based on their data availability for actual and future climate scenarios and on their location and elevation. The stations are listed and shown in Table B2 and in Figure B1.

Table B 1: List of the equations used for calculation of the potential evaporation.

Method	Equation	Needed variables	With:
Penmann-Monteith	$PET = \frac{0.408\Delta(R_n - G) + \gamma\frac{900}{T+273}u_2(e_s - e_a)}{\Delta + \gamma(1 + 0.34u_2)}$	Global radiation, daily temperature, relative humidity, daily mean wind velocity	R_n: net radiation at the crop surface (MJ $m^{-2}day^{-1}$), G: soil heat flux density (MJ $m^{-2}day^{-1}$), T: mean daily air temperature at 2 m height (°C), u_2: wind speed at 2 m height (m s^{-1}), e_s: saturation vapour pressure (kPa), e_a: actual vapour pressure (kPa), e_s- e_a: saturation vapour pressure deficit (kPa), Δ : slope vapour pressure curve (kPa °C), Γ : psychometric constant (kPa °C).
Hargreaves	$PET = 0.0023(T_{mean} + 17.8)(T_{max} - T_{min})^{0.5}R_a$	Mean, min, and max daily air temperature	T_{mean}: mean daily temperature (°C), T_{max}: daily temperature maximum(°C), T_{min}: daily temperature minimum (°C), R_a: extraterrestrial radiation (MJ $m^{-2}day^{-1}$).
Hamon	$PET = (\frac{N}{12})^2 \cdot e^{T/16}$	Mean daily air temperature	N: maximum possible hours of daylight on julian day (hr), T: mean daily temperature (°C).
Hamon WaSIM	$PET = (RG(1,1 - \propto) + 93 \cdot f_k)\frac{T+22}{150(T+123)}$	Mean daily air temperature	RG: global radiation (J $cm^{-2}day^{-1}$), α: albedo (-), f_k: empirical correction factor (-) - set to 0.5, T: mean daily temperature (°C).
Oudin	$PET = \frac{R_e T_a + 5}{\lambda\rho\ 100}$, if $T_a + 5 > 0$; PET=0 otherwise	Mean daily air Temperature	R_e: extraterrestrial radiation (MJ $m^{-2}day^{-1}$), λ: latent heat flux (MJ kg^{-1}), ρ: density of water (kg m^{-3}), T_a: mean daily temperature (°C).

In Figures B2 and B3 the calculated annual sums and mean monthly sums of PET are compared for the five calculation methods. As an indication, the actual evapotranspiration estimated based on the water balance for reference hydrologic catchments in Switzerland (HADES, Table 6.3) is also given for each station (Figures B1 and B3). This information is only given as an indication, as the HADES catchments have lower mean elevation than their corresponding closest weather station. Interesting are the large differences that can be observed between the different PET calculation methods. The PET comparison shows that the Hamon and Hargreaves equations give similar overall results and are closer to the FAO reference (Penmann-Monteith) than Oudin (which was used in the ASG1-project). Given these observations, the Hamon equation represents a good choice for the calculation of PET in our project, as it has the advantage to only need mean daily temperature as input data, which is available for the entire modeling period (for actual and future climate) as a gridded product. Global radiation, and wind speed or min/max temperatures are namely not available for the gridded products of

the future scenarios (Global radiation and min/max temperature are only available for the 13 weather stations for the future climate scenarios). This lack of data makes the use of the Penmann-Monteith or Hargreaves equations complicated for future climate. The Oudin equation shows on average too low PET compared to Penmann-Monteith.

Table B 2: List of the stations used for the comparison of PET-calculation methods.

ID	Station	Elev (m asl)	X (m)	Y (m)	River basin
SAM	Samedan	1709	787210	155700	Inn
COV	Piz Corvatsch	3302	783151	143522	Inn
SBE	San Bernardino	1639	734112	147296	Ticino
CIM	Cimetta	1661	704433	117452	Ticino
ABO	Adelboden	1327	609350	149001	Rhine
DAV	Davos	1594	783514	187458	Rhine
PIL	Pilatus	2106	661910	203410	Rhine
GUE	Guetsch ob Andermatt	2283	690050	167475	Rhine
SAE	Saentis	2502	744200	234920	Rhine
WFJ	Weissfluhjoch	2691	780615	189634	Rhine
MVE	Montana	1427	601706	127482	Rhone
GSB	Col du Gd St. Bernard	2472	579200	79720	Rhone
JUN	Jungfraujoch	3580	641930	155275	Rhone/Rhine

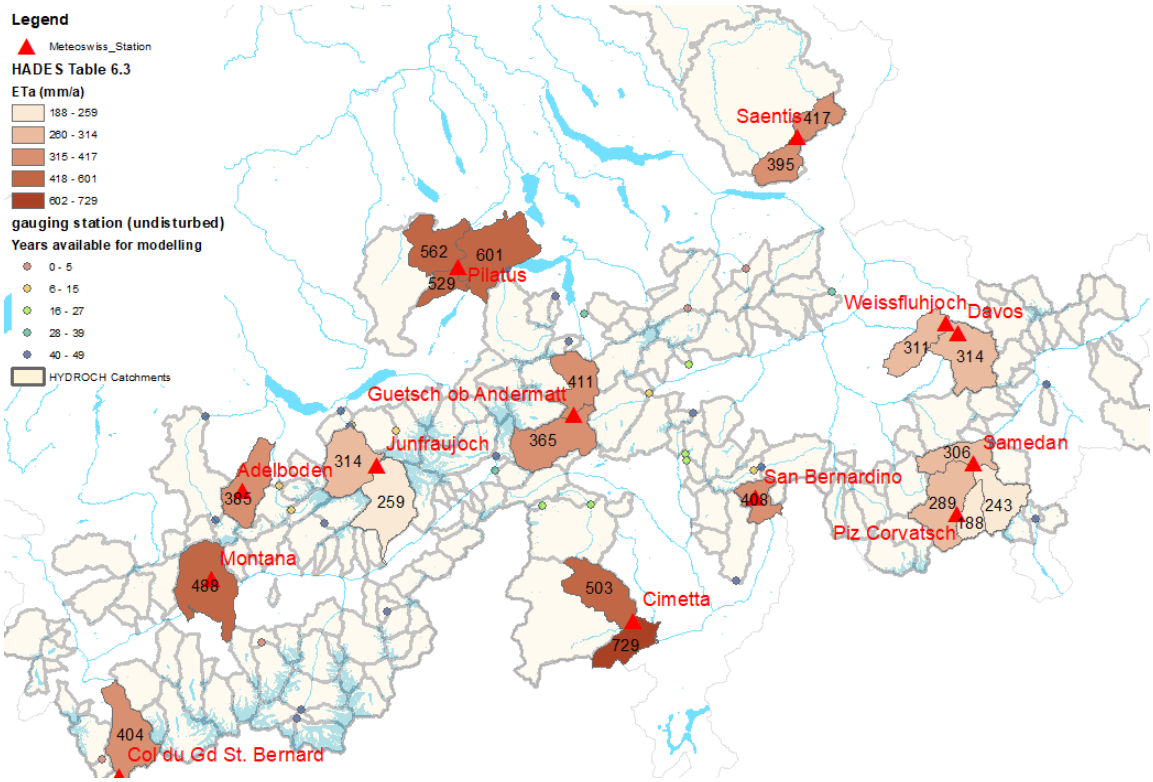

Figure B 1: Location of the meteorological stations used for the calculation of PET. PET from HADES table 6.3 is given for the closest reference catchment.

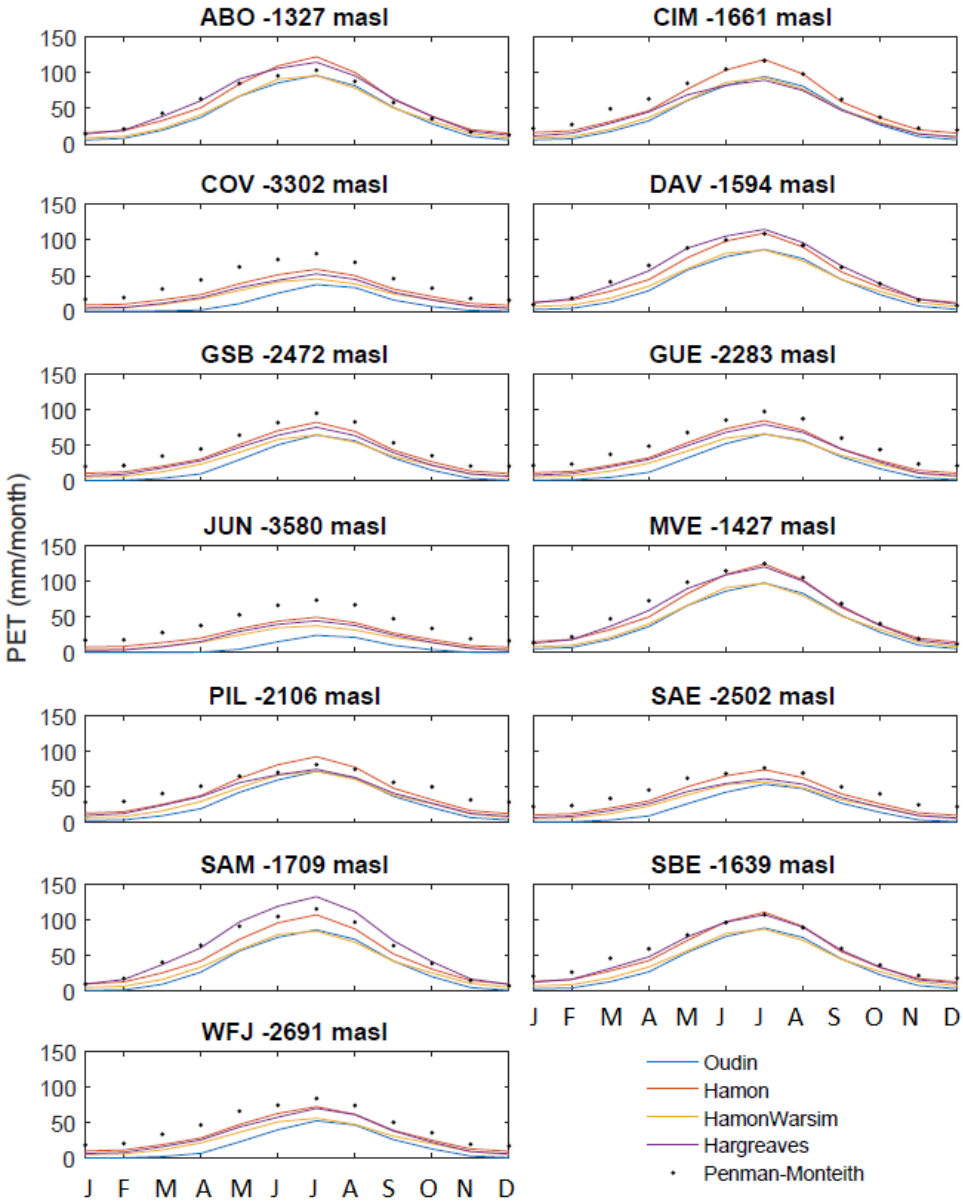

Figure B 2: Comparison of monthly mean PET calculated with 5 different methods for 13 meteorological stations (ca. 1970 – 2018).

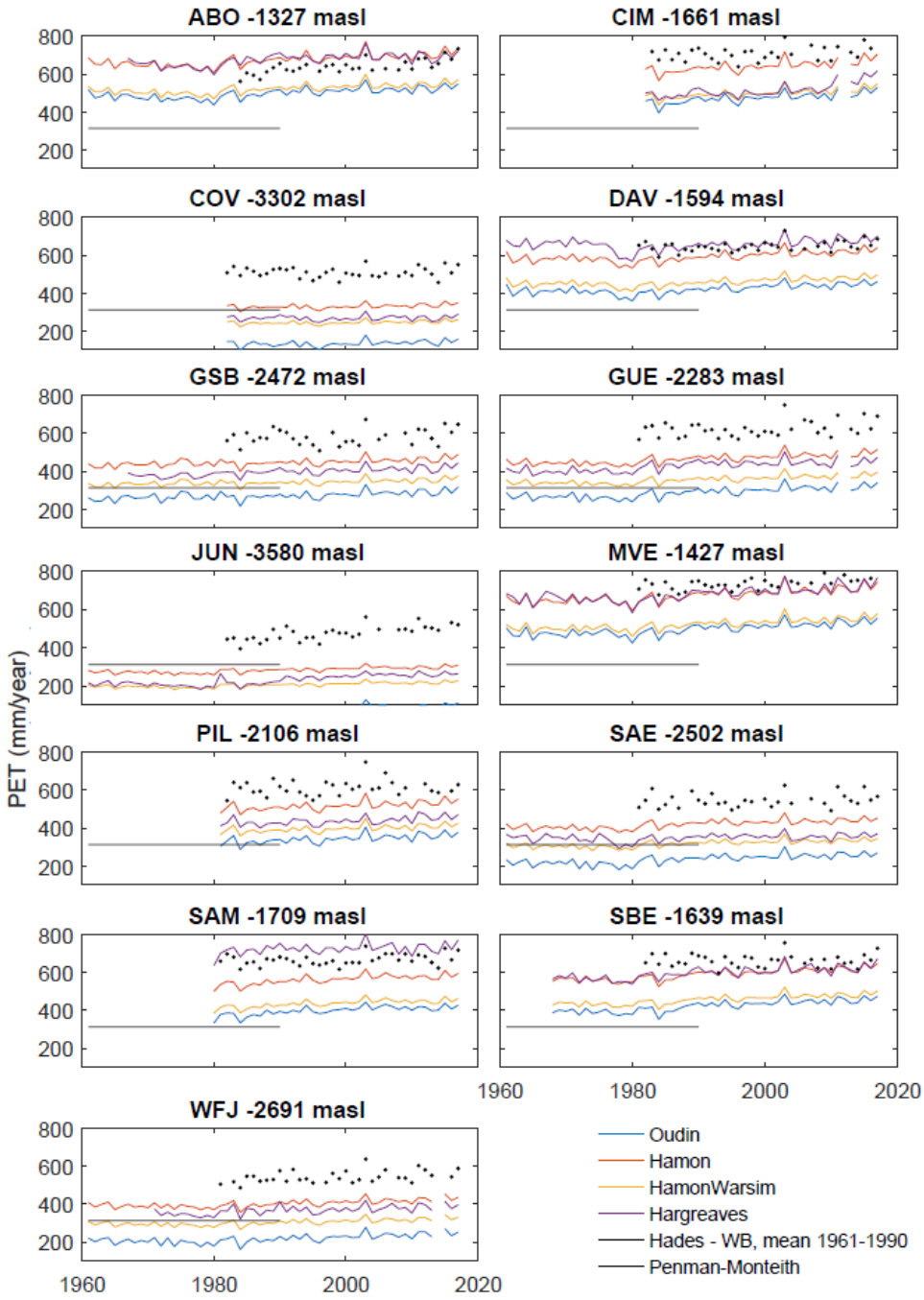

Figure B 3: Comparison of yearly mean PET calculated with 5 different methods for 13 meteorological stations (ca. 1970 – 2018).

In Figure B4, the trends of the PET were calculated at each weather stations. Trends of up to 28 mm/decades for the time period 1961-2018 were found. These results are comparable to the observations of Duethmann and Blöschl (2018) for alpine catchments in Austria (18 mm/decades on average). The observation of trends in the PET values supports the idea that time invariant PET values should not be used for long-term discharge modeling, especially in the context of climate change.

Based on the results of the PET calculation methods comparison, it was decided to use the Hamon equation to calculate PET in our project. Furthermore, daily PET values, instead of usual monthly sums averaged over the entire time period were chosen as input data for the HBV-light model, in order to assess for PET trends. PET was calculated from the gridded datasets RhiresD and TabsD for current and CH2018 for future climate for each headwater catchment.

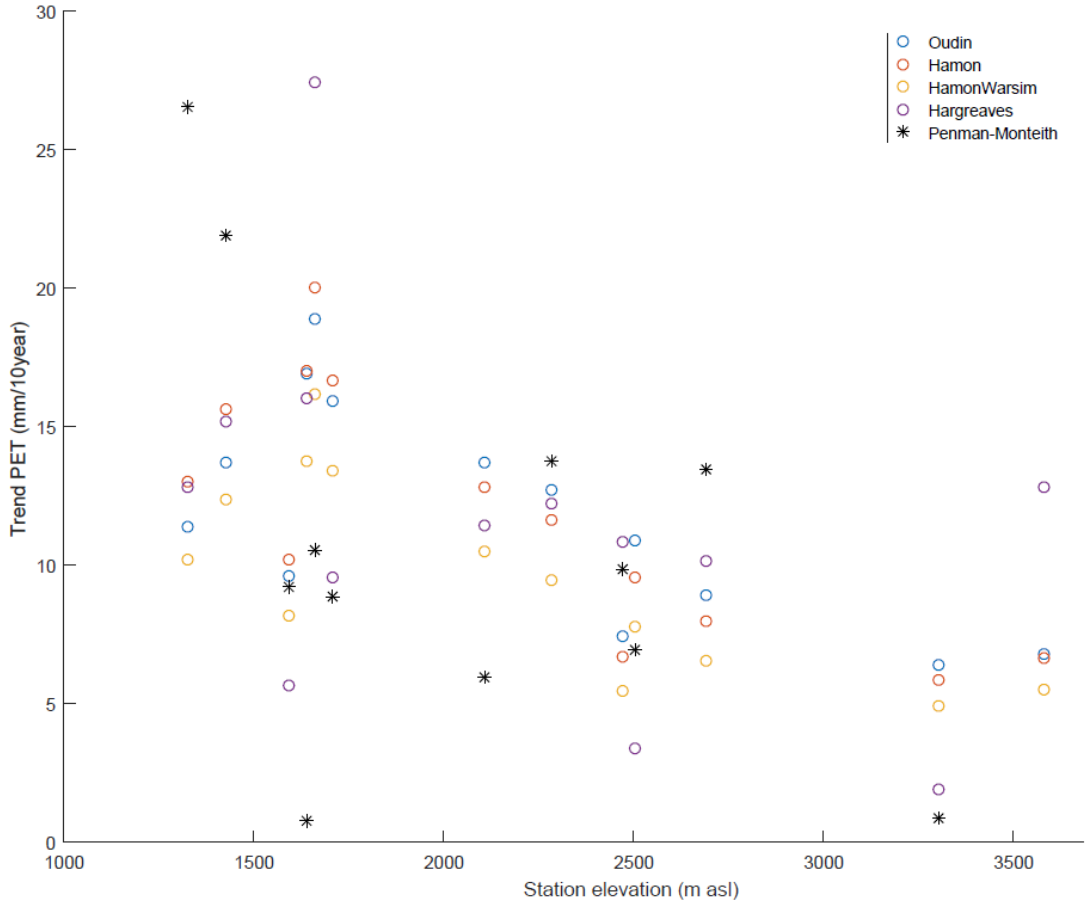

Figure B 4: Trend of PET calculated at each station for the time period ca. 1970 – 2018.

APPENDIX C: Multi-criteria calibration

C.1 Multi-criteria calibration of 38 gauged catchments (5 non-glacierized)

The gauged catchments were calibrated with the GAP-tool implemented in HBV-light on discharge, snow and glacier cover observations. To evaluate the calibration steps, a weighted objective function was used. The calibration procedures, the weights and the choice of the goodness of fit measures used for discharge, snow and glacier cover are based on previous analyses from the ASG1-project (Stahl *et al.*, 2016). In these analyses, the weight of each goodness of fit measure has been defined in a qualitative assessment through an iterative process, including several test simulations with different calibration settings and weights. For this study, we adapted the weighting on the quality of the observations available for the 38 gauged headwater catchments.

Discharge observations can be uncertain due to measurement issues (e.g. ice in the winter), to the data source (e.g. discharge derived from lake water level changes), or due to unknown disturbances upstream the gauge (e.g. water diversion and returns). Discharge measurements were considered as uncertain if they come from uncertain sources (e.g. see level changes, 2 catchments; see Table A1 in Appendix A), or if there is a large difference between the precipitation input (after correction) and the discharge data and it was not possible to make a clear statement on which data is more accurate (5 catchments). The efficiency measures were different for the catchments with reliable discharge observations (31) and uncertain discharge observations (7). In the first case, the calibration was weighted 50% on discharge, 30% on snow, and 20% on glacier observations (Eq. 2). Three different objective functions were used for discharge calibration in order to account for seasonality – high flow in summer assessed with the seasonal Nash-Sutcliffe Efficiency for the period June 1st to September 30th (weighted 15%) and low flow in winter assessed with the logarithmic Nash-Sutcliff Efficiency (weighted 15%) – as well as the volume assessed with the Lindström Efficiency (weighted 20%). In case the discharge measurements were uncertain, the calibration was weighted 30% on discharge with the Spearman Efficiency, 42% on snow and 28% on glacier obervations (Eq. 3). For the unglacierized catchments, the calibration was weighted 62% on discharge and 38% on snow observations (Eq. 4).

The weighted objective functions for the 38 headwater catchments with discharge observation records are:

a) for catchments with reliable discharge data:

$$R = 0.2 \cdot R_{Q1} + 0.15 \cdot R_{Q2} + 0.15 \cdot R_{Q3} + 0.15 \cdot R_{SCA} + 0.15 \cdot R_{SWE} + 0.2 \cdot R_G \quad (2),$$

b) for catchments with uncertain discharge data:

$$R = 0.3 \cdot R_{Q4} + 0.21 \cdot R_{SCA} + 0.21 \cdot R_{SWE} + 0.28 \cdot R_G \quad (3),$$

c) for non-glacerized catchments:

$$R = 0.24 \cdot R_{Q1} + 0.19 \cdot R_{Q2} + 0.19 \cdot R_{Q3} + 0.19 \cdot R_{SCA} + 0.19 \cdot R_{SWE} \quad (4).$$

Where

R	Weighted objective function used for parameter optimization
R_{Q1}	Lindstrom measure (discharge simulation)
R_{Q2}	Nash-Sutcliffe efficiency of logarithmic flow (discharge simulation)
R_{Q3}	Seasonal Nash-Sutcliffe Efficiency for flows from Jun-1 to Sep-30 (discharge simulation)
R_{Q4}	Spearman Rank (discharge simulation)
R_{SCA}	Root Mean Square Error (RMSE), performance criterion for the simulation of SCA
R_{SWE}	Mean Absolute Normalized Error (MANE), performance criterion for the simulation of SWE (up to 2500 m asl)
R_G	Absolute Mean Relative Error (AMRE), performance criterion for the simulation of glacier volume change

Where for all criteria R_i, the optimum (perfect fit) value is 1.

C.2 Parameter regionalization and multi-criteria calibration of the 157 ungauged catchments

For the ungauged headwater catchments, a regionalization approach was used. Each ungauged catchment received the calibrated model parameters from five gauged donor catchments (Figures 7 and 8). The five transferred parameter sets were then re-calibrated on SWE, SCA and glacier cover change observations using the GAP-tool implemented in the HBV-light model. Finally, the discharge was simulated with the five calibrated parameter sets and the ensemble mean was calculated for all discharge components as the average of the five discharge time series modelled by each of the five transferred parameter sets.

To find the five gauged donor catchments, catchments were compared based on their characteristics. These characteristics were divided into nine categories:

1) Distance between two catchments (km)
2) Catchment area (km^2)
3) Mean catchment slope (-)
4) Mean catchment Aspect (°)
5) Catchment elevation: mean (m asl), min (m asl), max (m asl) and elevation range (m; source: DHM25 Switzerland)
6) Glacier cover: relative glacier area (year 1973, %), change in glacier area ($A_{Glacier,\ 2010}/A_{Glacier,1973}$), mean glacier elevation (m asl), aspect (°), slope (°) and thickness (situation at year 1973, m water equivalent; source: DHM10 Switzerland and glacier data from Table 1)
7) Climatic characteristics: mean annual precipitation sum (mm), mean annual temperature (°C), rain/snow fraction (-), mean annual snow water equivalent (mm), mean precipitation and temperature gradients (%/100m, °C/100m), mean annual potential evapotranspiration (mm), mean 1°C elevation (m asl) and climatic water balance (P-PET, mm; source: Meteorological data RhiresD and Tabs, DHM25 Switzerland)
8) Regions:
    - Snow regions from SLF: 1 to 10 (category; source: HADES Table 3.3)
    - Alpine Region as defined by SLF: Inneralpine Gebiete, Oestlicher/Westlicher/Nördlicher/Zentraler Alpenhauptkamm, Ost, Süd, Transit (category; source: http://www.slf.ch/schneeinfo/zusatzinfos/interpretationshilfe/geographische_begriffe/alpenhauptkamm_d.gif)
9) Groundwater type: Mix CrCa, Carbonate, Cristalline, Mix CaMolasse, Mix CaEvaporikast, none (category; source: HADES Table 8.4)

The difference between all characteristics was calculated between each ungauged catchment and all gauged catchments. A mean value was calculated for each category. To rank the donor catchments, the nine categories were weighted equally. The catchments were ranked based on the total difference: the smaller the difference, the more similar are the catchments. An example can be found in Figure 7 for ungauged catchment nr 4141.

EZGnr	Distance	Area	Aspect	Slope	Elevation				Glacier							Meteo								Region		GW	weighted mean
4141	km	km2	°	-	mean	min	max	#	h/#	A	2010/1973	asp	hmin	h	slope	thick	P	T	S/R	SWE	dP	dT	PET	h1deg	WB	SLF	Alp		
4036	2	5	13	5	9	2	2	2	1	15	27	13	1	2	10	4	35	9	9	16	2	18	11	23	33	0	13	13	8.64
4032	10	1	13	9	12	3	1	4	18	2	21	0	3	6	11	16	12	15	8	15	26	34	17	15	8	0	13	13	9.45
4016	12	15	13	8	1	4	2	2	13	14	26	0	2	5	21	1	27	5	5	4	24	10	6	5	28	0	13	13	10.77
4033	1	24	13	20	14	5	1	4	1	5	12	13	2	10	18	17	8	14	18	1	36	23	16	24	4	0	0	13	11.27
2001	13	8	13	27	19	4	2	2	1	16	25	0	3	8	12	8	11	13	13	17	1	5	13	15	9	13	13	0	11.38
1006	5	12	13	7	3	1	1	2	15	17	30	0	4	15	7	18	36	8	1	20	3	35	3	20	35	13	13	13	11.69
1004	7	25	0	1	11	2	6	7	28	22	7	0	5	28	8	26	32	10	14	5	18	32	4	25	29	13	13	13	12.08
3001	22	7	13	25	8	5	2	3	5	7	24	13	2	22	5	2	2	6	2	27	23	27	7	7	1	13	13	13	13.23
1002	3	13	0	35	10	3	2	1	12	20	31	0	2	12	2	14	38	2	17	29	28	36	10	31	36	13	13	13	13.45
4019	35	9	13	6	15	7	1	7	3	1	3	13	2	16	33	32	20	3	15	2	20	16	1	9	17	13	13	13	13.68
3002	21	6	13	13	17	1	3	4	22	23	14	13	4	19	29	29	14	17	23	34	19	9	15	19	14	13	13	13	13.79
3006	38	18	0	18	6	1	2	3	7	19	29	13	1	18	24	5	24	4	6	37	16	7	8	28	26	13	13	0	13.86
1005	4	28	0	2	21	6	3	3	31	25	32	8	11	34	34	34	37	19	26	35	31	19	24	18	37	13	13	13	13.99
4030	11	22	13	37	2	6	1	7	6	11	4	13	2	21	4	6	9	21	4	7	17	13	21	17	13	0	13	13	14.64
2004	8	21	13	3	16	2	3	5	32	25	33	9	12	35	35	35	33	18	24	10	32	6	19	26	31	13	13	13	14.75
4006	31	3	13	26	4	4	3	7	19	10	17	13	3	1	28	28	22	7	11	12	14	3	5	4	21	13	13	13	14.84
3005	37	20	13	10	7	1	1	2	2	13	10	13	3	20	23	10	4	16	3	28	10	12	14	18	6	13	13	13	15.05
4012	9	29	13	21	30	9	2	8	8	12	22	0	7	25	27	13	16	29	29	11	30	30	29	21	20	13	13	0	15.11
2009	19	10	13	19	23	4	5	3	24	24	31	13	4	9	31	20	6	27	20	6	22	25	28	2	2	13	13	13	15.11
4018	18	2	13	28	31	10	4	7	17	8	8	0	3	30	20	15	31	32	31	23	29	29	33	18	25	13	13	13	15.67
4013	16	26	13	12	33	13	1	13	10	9	20	0	8	31	6	9	17	31	33	8	27	28	32	6	3	13	13	13	15.74
2010	29	19	13	16	18	1	1	2	2	21	28	0	1	23	17	12	21	25	19	13	25	2	27	11	22	13	13	13	16.12
4004	24	23	13	24	5	8	6	14	27	30	13	0	10	4	9	25	10	1	7	9	13	11	2	1	10	13	13	13	16.24
4017	17	16	13	36	20	7	2	6	9	6	9	13	6	26	15	21	1	24	16	21	21	22	23	14	5	13	13	13	16.33
4083	25	32	0	15	24	11	6	15	25	31	11	0	10	11	13	24	7	23	22	25	9	17	22	2	11	13	13	13	16.36
3003	30	14	13	23	13	3	5	8	21	27	6	13	5	24	1	22	15	11	21	14	34	24	9	22	12	13	13	13	16.9
4015	20	35	13	17	36	13	1	13	4	4	1	13	7	27	16	3	3	33	34	19	8	31	34	16	7	13	13	13	17.31
4037	6	11	13	32	34	8	3	6	35	25	36	12	15	38	38	38	29	36	35	32	33	21	36	13	32	0	13	13	17.4
4005	32	30	0	30	26	7	3	11	16	29	16	0	5	13	26	7	18	12	10	24	15	1	12	2	16	13	13	13	17.52
3009	33	4	13	22	27	2	7	10	20	26	15	13	1	32	30	27	30	28	28	30	5	4	25	12	27	13	13	13	17.65
2005	15	27	13	34	29	10	2	9	14	18	23	13	2	14	3	11	5	30	27	31	6	26	31	30	15	13	13	13	18.23
4020	28	31	0	31	22	11	7	16	26	28	5	0	10	7	19	19	19	20	12	22	12	15	20	6	19	13	13	13	18.25
3004	27	33	13	4	25	4	7	12	30	33	18	13	9	29	25	33	23	22	30	3	37	8	18	10	23	13	13	13	18.47
4011	26	34	0	29	28	12	6	16	23	31	11	0	10	3	14	23	13	26	25	26	4	20	26	3	18	13	13	13	18.57
3008	34	17	13	14	32	3	10	12	29	32	19	13	5	33	22	31	28	34	32	18	7	14	30	8	24	13	13	13	19.22
4010	36	36	13	11	35	10	1	10	11	3	2	0	2	17	32	30	26	35	36	33	11	33	35	15	30	13	13	13	19.69
4007	14	38	0	38	38	14	8	6	33	25	34	10	13	36	36	36	34	38	38	38	38	38	38	29	38	13	13	13	22.55
4009	23	37	0	33	37	13	9	4	34	25	35	11	14	37	37	37	25	37	37	36	35	37	37	27	34	13	13	13	22.63

Figure C 1: Example of the ranking of the donor catchments based on 9 categories for catchment nr. 4141.

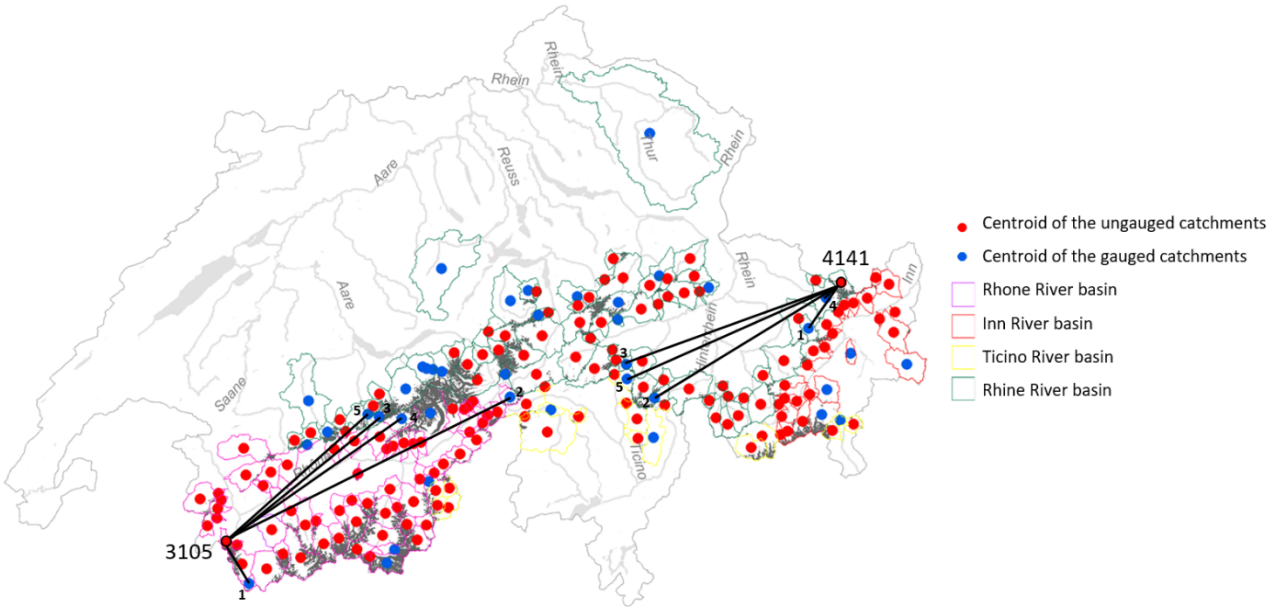

Figure C 2: Geographical representation of the five donor catchments for two ungauged catchments (nr 4141 and 3105) as an example for the regionalization method. The donor catchments are ranked from 1 to 5 depending on the catchment characteristic as shown in Figure 7.

The parameter sets of the five gauged donor catchments were transferred to the ungauged acceptor catchment. All ungauged catchments were then re-calibrated on snow and glacier cover information with the following weighted objective function:

$$R = 0.3 \cdot R_{SCA} + 0.3 \cdot R_{SWE} + 0.4 \cdot R_G \quad (5)$$

Where

R Weighted objective function used for parameter optimization

R_{SCA} Root Mean Square Error (RMSE), performance criterion for the simulation of SCA

R_{SWE} Mean Absolute Normalized Error (MANE), performance criterion for the simulation of SWE (up to 2500 m asl)

R_G Absolute Mean Relative Error (AMRE), performance criterion for the simulation of glacier volume change

Where for all criteria R_i, the optimum value is 1.

To test the regionalization algorithm, all gauged catchments were considered as ungauged and received five parameter sets from five donor catchments. This allowed us to assess how well the observed discharge could be represented with the regionalization approach. Example results for one catchment are shown in Figure D 1. Overall, we found that the discharge was well-simulated by the five parameter sets.

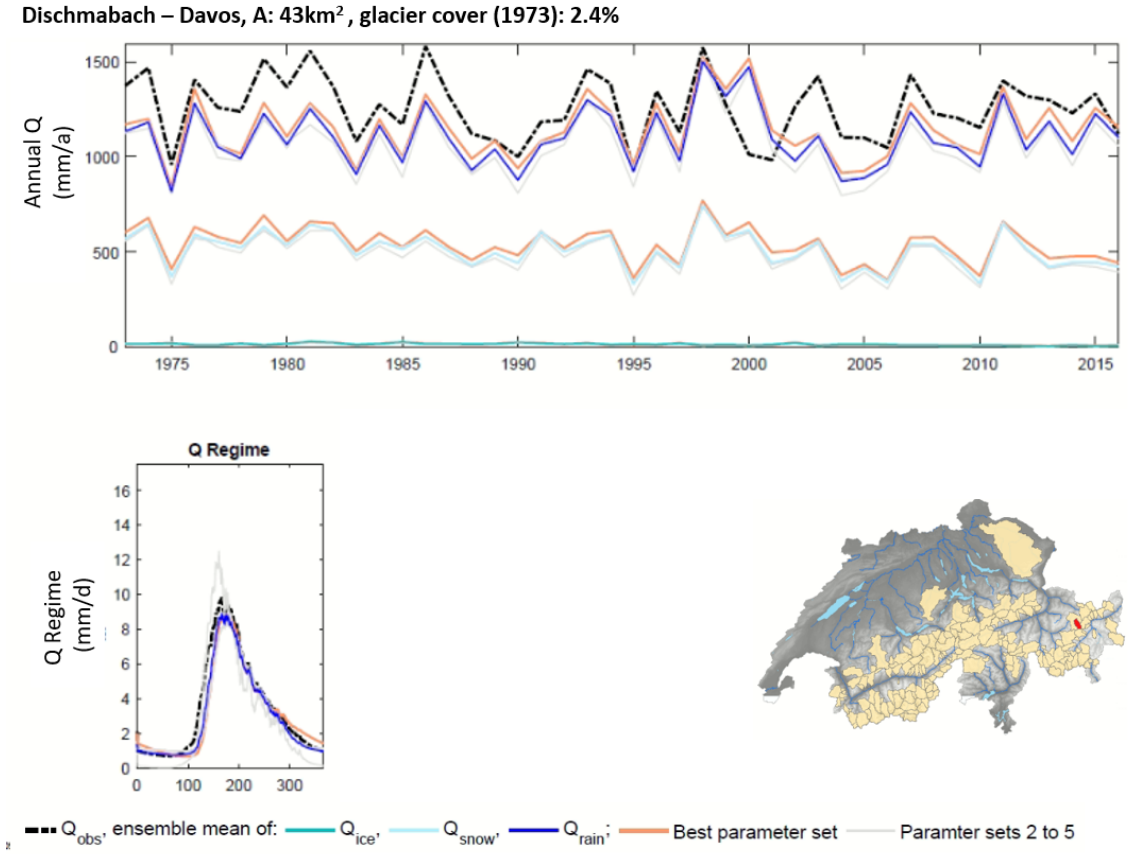

Figure C 3: Example of the regionalization approach applied on a gauged catchment.